AGU100 ADVANCING EARTH AND SPACE SCIENCE

Earth and Space Science

RESEARCH ARTICLE
10.1029/2019EA000781

Rawinsonde-Based Analysis of the Urban Boundary Layer in the Metropolitan Region of São Paulo, Brazil

Maciel Piñero Sánchez[1], Amauri Pereira de Oliveira[1], Ramón Pérez Varona[2], Janet Valdés Tito[1], Georgia Codato[1], Flávia Noronha Dutra Ribeiro[3], Edson Pereira Marques Filho[4], and Lucas Cardoso da Silveira[1]

[1]Department of Atmospheric Sciences, Institute of Astronomy, Geophysics and Atmospheric Sciences, University of São Paulo, São Paulo, Brazil, [2]Department of Experimental Physics, Institute of Physics, University of São Paulo, São Paulo, Brazil, [3]School of Arts, Sciences and Humanities, University of São Paulo, São Paulo, Brazil, [4]Interdisciplinary Center for Energy and Environment, Federal University of Bahia, Salvador, Brazil

Key Points:
- Main urban boundary layer features over the São Paulo megacity are estimated using 160 rawinsonde released in 2013 field campaigns
- Surface layer and entrainment layer thickness correspond to 10% (12%) and 16% (17%) of the urban boundary layer height in summer (winter)
- Four-year climatology of boundary layer height estimated objectively yield a maximum (1,632 m) in May and a minimum (1,061 m) in September

Correspondence to:
M. Piñero Sánchez,
maciel.sanchez@iag.usp.br

Citation:
Piñero Sánchez, M., de Oliveira, A. P., Varona, R. P., Tito, J. V., Codato, G., Ribeiro, F. N. D., Marques Filho, E. P., & Silveira, L. C. d. (2020). Rawinsonde-based analysis of the urban boundary layer in the metropolitan region of São Paulo, Brazil. *Earth and Space Science*, *7*, e2019EA000781. https://doi.org/10.1029/2019EA000781

Received 2 JUL 2019
Accepted 30 DEC 2019
Accepted article online 02 JAN 2020

Abstract The main features of the urban boundary layer in the metropolitan region of São Paulo are estimated based on rawinsondes carried out (a) every 3 hr in two 10-day field campaigns of the MCITY BRAZIL Project during the summer and winter of 2013 and (b) regularly once per day and continuously for 4 years from 2009 to 2013. On average, the boundary layer height showed a daytime maximum of 1476 ± 149 m in summer and 1122 ± 168 m in winter campaigns. The differences are related to seasonal variations in the (a) buoyancy flux at the surface, which was 30% larger in summer (4.7 ± 0.6 MJ m^{-2} day^{-1}), and the (b) static stability of the free atmosphere, which was 15% smaller in summer (3.3 ± 0.1 K km^{-1}). The average nighttime boundary layer height, estimated from equilibrium empirical expression, indicated maximum of 126 ± 13 m in summer and 122 ± 10 m in winter campaigns. The presence of a low-level jet was identified in 80% of the field campaign nights, with intensity varying from 2.7 to 14 m s^{-1} and height ranging from 95 to 962 m. The nighttime residual-mixing layer is well estimated using the air temperature gradient method and is a good indication of the maximum vertical evolution of the previous daytime boundary layer. The monthly average maximum boundary layer height varied from a minimum of 1,061 ± 77 m in September to maximum of 1,632 ± 96 m in May.

1. Introduction

Planetary boundary layer (PBL) properties over urban areas have received much attention from the research community lately in view of the fact that the worldwide urbanization process has increased the demand for resources to mitigate adverse effects on urban climate (Huang et al., 2017; Seidel et al., 2010; Zhang et al., 2014). Identified as the turbulent atmospheric layer adjacent to the surface, the PBL responds to surface variations within time scales smaller or equal to one hour (Stull, 1988; Wyngaard, 2010). As a consequence, the PBL properties vary in time and space in a very complex way. For undisturbed conditions and over horizontally homogeneous, flat, and continental regions, the PBL depth varies from hundreds of meters (typically from 50 to 300 m) during nighttime to a few kilometers (typically from 1 to 2 km) during daytime (Guo et al., 2016; Oke, 1987; Quan et al., 2013; Stull, 1988; Wyngaard, 2010).

Over an urban region, as the case of the Metropolitan Region of São Paulo (MRSP), the vertical structure of the PBL is modified by the presence of the urban canopy (Barlow, 2014; Bornstein, 1987). In general, urban land use intensifies turbulence and heat inputs to the atmosphere. As consequence, the so-called urban boundary layer (UBL) is deeper and warmer than the PBL over adjacent rural areas (Barlow, 2014; Barlow et al., 2015; Pal et al., 2012). Urban land use increases surface aerodynamic roughness, thus reducing horizontal wind speed. It also alters significantly surface energy and moisture budgets, producing energy surpluses and moisture deficits that induce positive anomalies of temperature (urban heat island) and negative anomalies of specific humidity (urban dry island). These surface modifications propagate upward as the UBL interacts with the surface, generating a very complex turbulence structure that reflects the overlapping of several internal boundary layers (Barlow, 2014; Bornstein, 1987; Oke, 1987). In addition to its scientific relevancy, knowing the behavior of the UBL has important practical applications in improving the performance of operational weather and climate models at regional scales and their applications to thermal comfort and air pollution assessments in urban areas (Garratt, 1994; Guo et al., 2016; LeMone et al., 2012; Liu & Liang, 2010; Seibert et al., 2000; Wang & Wang, 2016; Zhang et al., 2014).

The UBL properties of cities located in tropical and subtropical areas are less known than in higher latitudes. This is a critical issue for Brazil because the urban fraction of its population is expected to grow from the current 85% to over 90% by 2050 (UNESCO, 2017). To aggravate this problem, very little is known about the UBL properties of Brazilian cities. There are only two observational works available in the literature regarding the PBL in the MRSP (Landulfo et al., 2010; Nair et al., 2004). Observations carried out by Nair et al. (2004) using a Doppler sodar on 27 July 1999 indicated that during nighttime the surface-inversion (SI) layer reached 270 m and the low-level jet (LLJ) occurred at 1,300 m with a maximum wind speed of 21 m s^{-1} from the northeast. During daytime, the PBL height reached 1,600 m, and as the cold front moved in, it was substituted by a SI layer of 200 m. The observations using lidar by Landulfo et al. (2010), between July and September of 2007, indicated daytime maximum PBL height in São Paulo vary between 1,000 and 3,500 m.

The most common way to estimate the height of the PBL, which will be pursued in this work, is by visual inspection of vertical profiles of potential temperature, specific humidity, wind speed, and direction, which are generally provided by rawinsondes (Seibert et al., 2000; Seidel et al., 2010; Wang & Wang, 2016). Hereafter called the subjective method, it consists of visually comparing the observed structure with the expected behavior, using as a reference the vertical structure observed under undisturbed conditions as observed during a cloudless day over horizontally homogeneous land surface and flat topography. For this situation, under convective conditions, the PBL height is estimated as the level where the vertical gradient of potential temperature reaches the first relative maximum (Feng et al., 2015; Garratt, 1994; Hennemuth & Lammert, 2006; Oke, 1987; Seidel et al., 2010; Sorbjan, 1989; Stull, 1988). Alternatively and complementarily, the PBL height can also be estimated as the level where the vertical gradient of specific humidity (relative humidity and refractivity) reaches a relative minimum (Basha & Ratnam, 2009; Hennemuth & Lammert, 2006; Seidel et al., 2010; Wang & Wang, 2016). It is important to emphasize that besides PBL height, visual inspection of vertical profiles allows one to identify several other PBL properties, including the depths of surface layer (SL), mixing layer (ML), entrainment layer, and residual-mixing layer (RML).

Under stable and undisturbed conditions, the PBL height can be estimated by subjective method as the top of the SI layer (Coulter, 1990; Pournazeri et al., 2012; Seidel et al., 2010; Wang & Wang, 2016; Yu, 1978). Alternatively, the PBL height during nighttime can also be identified as the height of the nocturnal LLJ (Melgarejo & Deardorff, 1974; Oliveira et al., 1998; Zhang et al., 2014). In both cases, it is necessary to have vertical profiles of temperature and wind speed with high vertical resolution (almost equal to a few tens of meters), which is not the case for most of rawinsondes carried out regularly at upper air station networks worldwide. Another possibility, when vertical profiles of temperature and wind speed are not available or available with too-coarse resolution, which will also be pursued in this work is using turbulence measurements at the surface to estimate characteristic scales of SL turbulence, mainly friction velocity and Obukhov length scales, to estimate the PBL height employing empirical expressions. These empirical expressions based on the combination of characteristic scales of turbulence have been applied by different authors with relative success to estimate the height of the PBL during nighttime (Koracin & Berkowicz, 1988; Mahrt et al., 1982; Nieuwstadt, 1981; Seibert et al., 2000; Zilitinkevich, 1972; Zilitinkevich et al., 2007). The problem with these expressions is that they are valid for equilibrium conditions and require previous validation. Moreover, the characteristics scales of turbulence are very difficult to estimate, especially in areas with complex topography and heterogeneous land use.

The height of the PBL can also be estimated by remote sensing systems, such as sodars (Beyrich, 1997; Seibert et al., 2000), lidars (Banks et al., 2015; Compton et al., 2013; Dang et al., 2019; Hennemuth & Lammert, 2006; Hicks et al., 2015; Huang et al., 2017; Landulfo et al., 2003; Liu et al., 2018; Sawyer & Li, 2013), wind profiler radars (Liu et al., 2019; Quan et al., 2013; Wyngaard, 1990), and ceilometers (Emeis et al., 2004; Lotteraner & Piringer, 2016). Even though remote sensing systems yield a continuous description of the PBL height, comparatively to rawinsonde is limited to much more restricted geographical coverage. Therefore, it will take considerable time and resources to reach a similar worldwide coverage, mainly in developing countries like Brazil. Besides, in the case of lidar system the accuracy of the algorithms deployed to retrieve PBL properties are limited to the daytime convective boundary layer (CBL) height because detection systems are highly sensitive to thermal stability. Most systems yield good results only for strong thermal convection conditions. When turbulence is not so strong the heterogeneity in the vertical distribution of

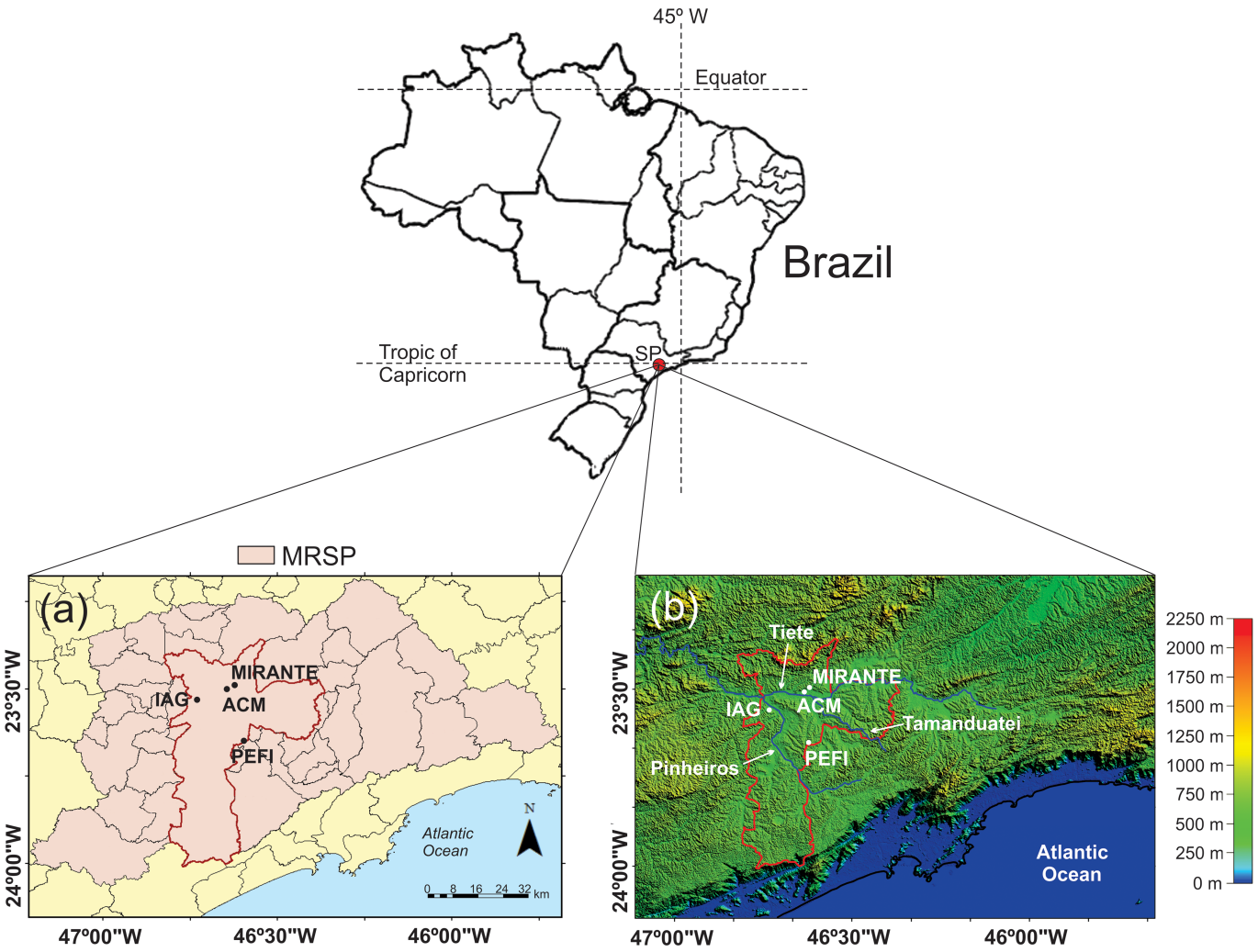

Figure 1. (a) Geographic features of the MRSP. (b) The city of São Paulo is indicated by red borders. All the remaining 38 cities are also indicated. The observation sites are indicated by IAG (Institute of Astronomy, Geophysics and Atmospheric Science), ACM ("Campo de Marte" Airport), PEFI ("Parque Estadual Fontes do Ipiranga"), and MIRANTE ("Mirante de Santana"). Topography is based on the highest-resolution topographic data (3-arc-second resolution—90 m) generated from NASA's Shuttle Radar Topography Mission (SRTM), available online (https://www2.jpl.nasa.gov/srtm/).

aerosol concentration and the presence of multilayer of aerosols reduce considerable the performance of these algorithms (Liu et al., 2018). In addition, lidar retrieving of the stable boundary layer (SBL) height is greatly hampered by the blind zone near the surface induced by the overlap errors (Dang et al., 2019).

The main objective of this work is to characterize the vertical structure of the UBL in the MRSP using rawinsondes carried out every three hours for two 10-day field campaigns of the MCITY BRAZIL Project. This characterization is complemented using rawinsondes carried out regularly twice a day over four years at the "Campo de Marte" Airport (ACM) of São Paulo City. The MCITY (MegaCITY) BRAZIL Project was designed to fill observational gap by assessing the urban effects on the climates of the major Brazilian cities (Oliveira et al., 2019). The materials and data set are presented in section 2. Methods used to estimate the UBL properties are described in section 3. UBL properties are discussed in section 4. The results are summarized in the conclusion.

2. Materials and Data

2.1. Experimental Area

The MRSP is located close to the Tropic of Capricorn in the "Paulista" plateau at 722 m above sea level (asl) and 65 km from the Atlantic Ocean (Figure 1). It is a conurbation of 39 cities (Figure 1a) with a population of

21.7 million habitants and 13.2 million vehicles (IBGE, 2019). São Paulo City occupies the core region of the MRSP and, with a population of 12.2 million habitants, is Brazil's largest city. It became a megacity in the early 1990s. The topography of the MRSP is complex (Figure 1b), which makes very difficult to isolate its effects on the surface circulation from the ones induced by the land use (Oliveira et al., 2003). The entire urban portion of the MRSP is located in the "Paulista" plateau, limited at the north and northwest by a chain of ridges varying from 300 to 700 m high. The MRSP is characterized by three major river valleys: the "Tiete" River valley, oriented in the east-west direction; the "Tamanduatei" River valley, oriented in the northwest to southeast direction; and the "Pinheiros" River valley, oriented in the northeast to southwest direction. In the south, there are large bodies of water composing the Billings Dam system, which occupies 582.8 km^2.

2.2. Climate

In general, the climate characterizations of the MRSP cities are based on meteorological surface stations located in the south (PEFI: 23°39′04″S, 46°37′20″W, 799 m asl) and north (MIRANTE: 23°29′47″S, 46°37′11″W, 792 m asl) portions of São Paulo City (Figure 1). Alvares et al. (2014) has analyzed all the data available in the MRSP area, including those of PEFI and MIRANTE, and concluded that according to the Köppen classification, the climate of São Paulo City can be classified as high elevation subtropical humid (Cwb). Indeed, considering the PEFI and MIRANTE data set (Figure 2), the São Paulo climate is characterized by a dry mild cold winter with monthly mean temperatures varying from minima of 15.3 °C (PEFI) and 15.8 °C (MIRANTE) in July, and a wet and warm summer with maxima of 22 °C (PEFI) and 22.4 °C (MIRANTE) in February (Figure 2a). During winter the minimum specific humidity is 9.1 g kg^{-1} in July and during summer the maximum is 14.6 g kg^{-1} in February in both PEFI and MIRANTE (Figure 2b). During winter the minimum precipitation occurs in August and varies from 40.5 mm (PEFI) to 39.6 mm (MIRANTE). During summer the maximum precipitation occurs in January and varies from 223 mm (PEFI) to 237 mm (MIRANTE) (Figure 2c).

The MRSP is characterized by weak surface winds throughout the year, with speeds varying from minima of 1.7 m s^{-1} (PEFI) and 2.3 m s^{-1} (MIRANTE) in May, to maxima of 2.3 m s^{-1} (PEFI) in December and 3.1 m s^{-1} (MIRANTE) in November (Figure 2d). These seasonal variations are controlled by the position of the semimigratory South Atlantic subtropical high and by the influence of South America continental low-pressure systems. The seasonal variations in the positions and intensities of these large-scale systems induce north to northeast winds during the summer and northeast to east winds in winter in São Paulo. These patterns are often affected by the passage of cold fronts, which penetrate the MRSP more frequently in association with strong to moderate prefrontal northwest winds and moderate to light postfrontal southeast winds (Garreaud & Wallace, 1998; Oliveira et al., 2003). The MRSP is also affected by mesoscale circulations such as sea breeze and local-scale circulations associated with topographic (mountain-valley and channeling) and land use (urban heat island and spatial variations in surface roughness) effects (Oliveira et al., 2003).

Considering air temperature and specific humidity from 1997 to 2018, precipitation from 1999 to 2018 and wind speed from 2010 to 2018 measured at IAG (details in section 2.3.2), it is possible to infer that local climatic features of IAG do not differ much from the climate characterized by PEFI and MIRANTE (Figure 2). Based on this similarity, it is assumed that turbulent fluxes (mainly buoyancy and momentum) measured at IAG can be used as representative of São Paulo City. This will allow us to use turbulence measurements at IAG to explain the behavior of the diurnal evolution of UBL (see section 4.3.3) and to estimate the UBL height during the stable regime (see section 3.3).

The analysis of rawinsonde data obtained during the field campaigns of February and August of 2013 provides information about the behavior of UBL representative of summer and winter conditions in the MRSP (Figure 2). The mean air temperature at IAG during both field campaigns in 2013 did not differ much of the normal values for the MRSP (Figure 2a). The specific humidity and wind speed were respectively slightly lower and higher (Figures 2b and 2d). Similar pattern was observed for the period of the regular rawinsonde data (2009–2013). During this period the accumulated rain was higher than normal on April and June and lower in May and August (Figure 2c).

2.3. Observations

The data used in this work are composed of two sets of vertical profiles of temperature, relative humidity, wind speed, and direction obtained from

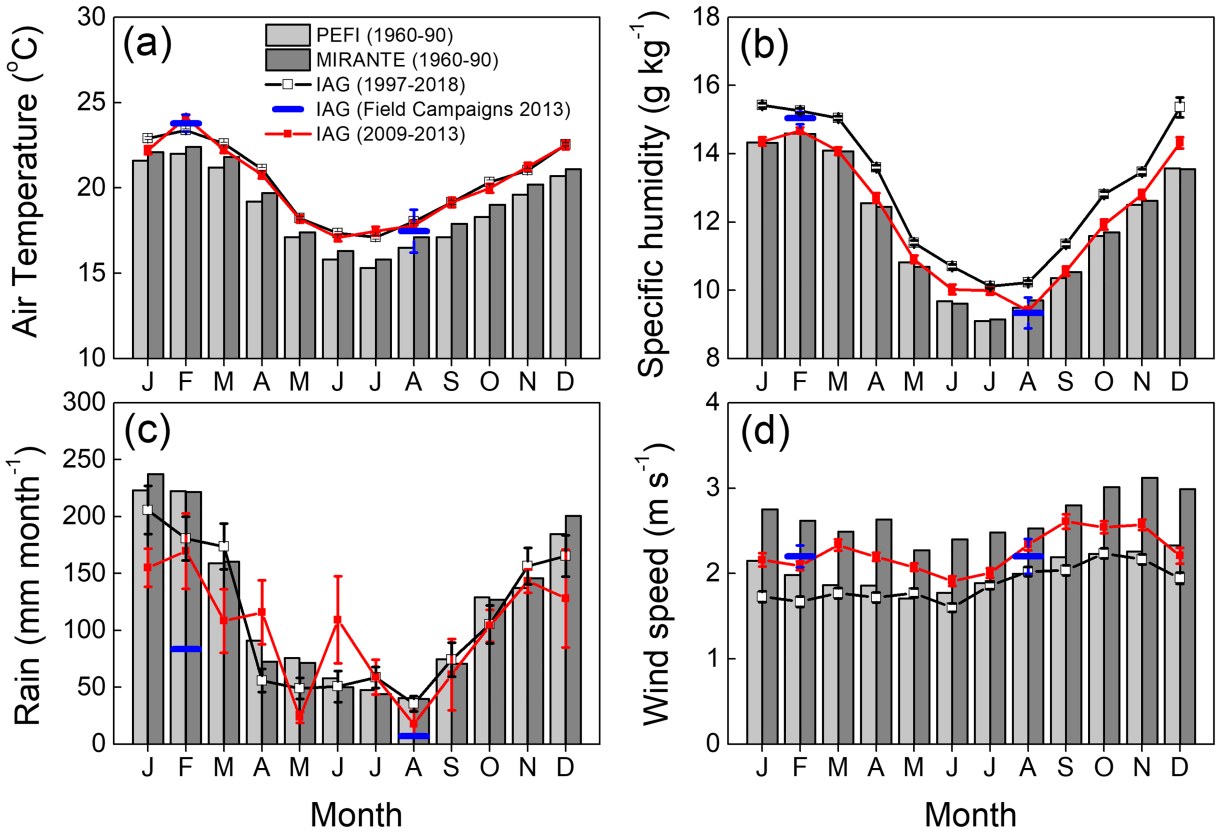

Figure 2. Seasonal variations in (a) air temperature, (b) specific humidity, (c) rain, and (d) wind speed observed at the meteorological surface station PEFI, MIRANTE, and IAG. Field campaigns values (blue horizontal bar) correspond to 10-day average (a, b, and d) and accumulate (c) during February and August 2013 at IAG and PEFI. The 2009–2013 mean values (red solid circle continuous lines) correspond to observations at IAG during the period of regular rawinsonde at ACM. Observation periods in IAG started in 1999 for rain (c) and in 2010 for wind speed (d).

a 160 rawinsondes carried out from 19 to 28 February and from 6 to 15 August every 3 hr and starting at 2100 LT (0000 GMT) as part of the 2013 summer and winter field campaigns of the MCITY BRAZIL Project (Oliveira et al., 2019); and

b 1,300 rawinsondes performed daily at 2100 LT for four years from 1 September 2009, to 16 August 2013.

This analysis is complemented by hourly values of turbulent buoyancy flux and friction velocity and Obukhov length estimated using the eddy covariance method based on observations of the wind speed components, air temperature, and water vapor density measured with a sampling rate of 10 Hz, 25.4 m above the surface from 19 to 28 February and from 6 to 15 August.

2.3.1. Soundings

All the soundings described above were performed at the ACM (23°30′32″S, 46°38′04″W, 722 m) using an upper air rawinsonde system manufactured by Vaisala, Inc. This system is comprised of a DIGICORA III data acquisition system and radiosonde model RS92-GSP, manufactured by Vaisala Inc., Finland, which were set up to perform soundings with sample frequency of 0.1 Hz during the MCITY BRAZIL Project field campaigns. Before 2012, all soundings performed daily used a DIGICORA II data acquisition system and model RS92 radiosonde. According to the manufacturer, the RS92 family radiosonde accuracy is 0.5 °C for air temperature, 5% for relative humidity and 1 hPa for pressure. The uncertainty in wind velocity is 0.l5 m s^{-1} and that for wind direction is 2°. A ground-check procedure was carried out using a surface meteorological station from the ACM as the ground reference. All soundings used a 30-g balloon that was inflated to offset the payload of 150 g (radiosonde and parachute) to sustain an initial ascent speed of 5.5 m s^{-1}. Variation in the drag force caused by turbulent motions in the PBL and balloon expansion alters the ascent speed (Johansson & Bergström, 2005). Taking into consideration these effects the actual error for wind speed and direction becomes 1 m s^{-1} and 5°, respectively (WMO, 2006).

The vertical resolution of the soundings carried out at ACM, which was estimated as the vertical distance between two consecutive measurements points from surface to 4,000 m, are indicated in Figures 3a and 3b. It is noticeable that the resolution of the soundings launched during the field campaigns in 2013 (Figure 3a) were finer than the soundings launched regularly from 2009 to 2013 (Figure 3b). During the field campaigns, the most frequent resolution was 61–70 m for both daytime and nighttime soundings (corresponding to 51% and 59% of the cases, respectively). For the regular soundings, the most frequent resolution was 301–350 m (corresponding to 53% of the cases).

The spatial representativeness of the soundings can be accessed from the trajectories of the balloons in the first 4,000 m after release. The trajectories of all rawinsondes during both field campaigns in 2013 are indicated in Figures 3c and 3d. The positions of the balloons at 4,000 m, which are indicated by solid red circles, show that all the soundings were located within the urban limits. This indicates that the PBL properties described in this work from these rawinsondes are representative of the UBL of the MRSP as long as balloons and air mass trajectories coincide. This hypothesis is not totally satisfied near to the surface, where topography and land use are likely to cause significant changes in the wind field. This effect can be more pronounced near to the urban boundaries. However, in the case of a very large urban area like the MRSP, it seems plausible to assume that most of rawinsondes are sampling urban air because the launching point (ACM) is located in the urban area at approximately 7 km far from the urban border (estimated as the radius of the white circle in Figure 3c). Besides, all balloon trajectories are located way from the urban border as indicated by white circles in Figures 3c and 3d. One way to check these assumptions is performing a footprint assessment similar to the ones carried out for sensors fixed at the surface (Leclerc & Foken, 2014).

2.3.2. Turbulence and Conventional Meteorological Variable

The turbulence measurements, corresponding to three wind components (u, v, and w), sonic temperature (Ts), and water vapor density (ρ_{H20}) were carried at the IAG micrometeorological platform (IAG) using a 3-D sonic anemometer coupled to a gas analyzer, model IRGASON, manufactured by Campbell Scientific Inc., USA. This sensor was installed at 8.4 m on a 10-m tower located at the center of concrete platform at the top of a four-story building at 17 m above the surface, achieving a total height of 25.4 m above the ground level (agl). The IAG building is located on the University of São Paulo campus (23°33′34″S, 46°44′01″W, 744 m asl) on a relatively flat area characterized by suburban land use located in the west portion of São Paulo City (Figure 1). A more complete description of the methodology used to estimate vertical turbulent fluxes can be found in Oliveira et al. (2019). The quality control procedures adopted is based on Vickers and Mahrt (1997) and Aubinet et al. (2012), and only 60% of the original series were considered valid. It includes also a technique to detect and remove building distortion in the flow (Fortuniak et al., 2013). The mean building height in the circular area of 500-m radius (centered at IAG) is 7.0 m, indicating that turbulence measurements performed at IAG (25.4 m agl) are likely to be sampling turbulence in the inertial layer.

Conventional meteorological variables used in this work were also measured at IAG. They correspond to 5-min average air temperature and relative humidity, measured from 1997 to 2018, horizontal wind speed from 2010 to 2018, and precipitation from 1999 to 2018. These variables were continuously measured with sample frequency of 0.5 Hz in the micrometeorological platform of IAG simultaneously at 18.7 m agl (air temperature, relative humidity, and precipitation) and at 26.5 m agl (wind speed). It was used temperature and relative humidity sensors manufactured by Vaisala, models HPM35A (1996–2008), HPM35C (2009) and manufactured by Campbell Scientific Inc. model CS215 (2010–2018); Tipping bucket rain gauges manufactured by Campbell Scientific Inc., models TE525 (1997–2012) and TB4 385 (2013–2018), and a cup anemometer and vane manufactured by MetOne Instruments Inc., model 034B (2010–2018). Quality control procedure was applied to these measurements so that glitches and other problems were removed using a filtering algorithm based on running median (Velleman & Hoaglin, 1981). Discontinuities in the time series of these meteorological variables caused by sensor substitutions were detected and removed using as reference offsets estimated by running side by side the sensors involved in the change.

3. Methodology

In this work, three methods are used: the subjective method, objective method and empirical method. To characterize the vertical structure of the UBL in the MRSP, it was used a subjective method based on visual inspection of vertical profiles of potential temperature, specific humidity, wind speed, and direction from

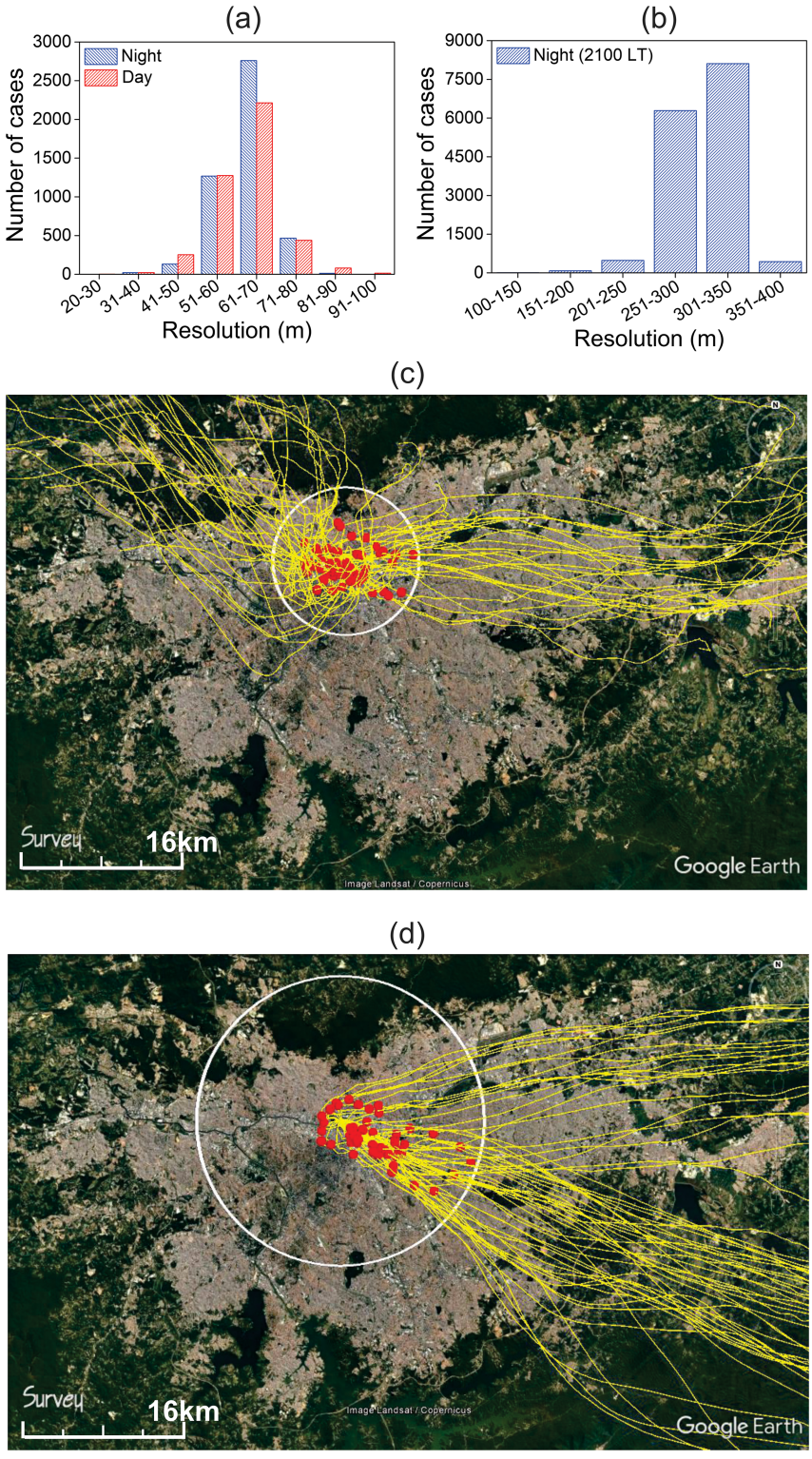

Figure 3. Frequency distribution of vertical resolution in the first 4,000 m for the (a) 160 rawinsondes carried out in February and August of 2013 and the (b) 1,300 rawinsondes carried out between September 2009 and August 2013. The trajectories (yellow lines) describe the rawinsondes during the field campaigns for (c) 19–28 February 2013 and (d) 6–15 August 2013, at the ACM, São Paulo. The white circles indicate the farthest positions in the *X-Y* plane by the balloon upon reaching 4000 m above the surface (red dots) (Google Earth). In (c) and (d) white circles radius are 7 and 14 km. Vertical resolution of the sounding in (a) and (b) corresponds to the vertical distance between two consecutive measurements points.

fine-resolution rawinsondes carried out every three hours during two 10-day field campaigns of the MCITY BRAZIL Project in February (summer) and August (winter) of 2013. This characterization was complemented by describing the seasonal variation of the maximum daytime UBL height estimated from coarse-resolution rawinsondes carried out regularly twice a day over 4 years, from 1 September 2009 to 16 August 2013 using objective method. The empirical method was used to estimate the nighttime UBL height during the field campaigns of the MCITY BRAZIL Project.

3.1. Subjective Method

The subjective method can generally be defined as the visual comparison of observed vertical profiles of potential temperature, specific humidity, wind speed, and direction provided by rawinsondes of the atmosphere with expected or idealized behavior (Sánchez, 2017; Seibert et al., 2000; Seidel et al., 2010; Wang & Wang, 2016). In this work the thermodynamic and dynamic structures observed during daytime convective and nighttime stable regimes on 8–9 August 2013 were chosen as a reference to apply the subjective method in the MRSP (Figure 4). During that day, undisturbed synoptic conditions characterized by cloudless skies prevailed in the MRSP.

During daytime, the thermodynamic properties of the CBL were identified in this work using the vertical profiles of potential temperature and wind speed observed at 1500 LT on 8 August as a reference (Figures 4a and 4b). In the vertical profile of potential temperature (Figure 4a), three adjacent layers can be identified: the SL as the shallow layer adjacent to the surface where the potential temperature decreases (superadiabatic layer), the ML where potential temperature is constant, and the entrainment layer where potential temperature increases with height at a rate larger than in the free atmosphere immediately above. The entrainment layer coincides with the upper inversion layer. Based on this vertical structure, we identify the height of the SL by Z_S and the thickness of the ML and entrainment layer by h and h, respectively. The height of the CBL is indicated by Z_{CBL} and corresponds to the bottom of the entrainment layer and includes the SL and ML such that $Z_{CBL} = Z_S + h$. The bottom, top, and inversion strength of the entrainment layer are indicated by Z_i, Z_T, and θ/h, where $\theta = \theta\,(Z_T) - \theta\,(Z_i)$. The vertical gradient of potential temperature in the free atmosphere is indicated by γ_θ. Potential temperatures at the surface and in the ML are indicated by θ_0 and θ_M, respectively. The turbulent vertical mixing on that day was strong enough to homogenize wind speed (Figure 4b) and maintain a three-layer pattern similar to the potential temperature (Figure 4a) and mixing ratio (not shown).

During nighttime, the thermodynamic and dynamic properties of the SBL and the RML were estimated considering the vertical profiles of potential temperature and wind speed observed at 2100 LT on 9 August as a reference (Figures 4c and 4d). The SI layer can be identified in the potential temperature profile (Figure 4c). The height of the SI layer top is identified by Z_{SI}. The SI layer strength is estimated by θ_{SI}/Z_{SI}, where $\theta_{SI} = \theta\,(Z_{SI}) - \theta_0$. The heights of the bottom (Z_{SI}) and top (Z_{RML}) of the RML, which corresponds to what remains of the daytime ML, can be identified visually for the nighttime period (Figure 4c). During nighttime, the presence of LLJ was determined considering the typical dynamic structure indicated in the Figure 4d as a reference. The wind speed and direction of the LLJ are indicated by V_{LLJ} and D_{LLJ}, respectively. The height of the LLJ is indicated by Z_{LLJ}. In this study a LLJ event occurs when the maximum wind speed $\geq$2.0 m s^{-1} is located in the first 1,000 m and is 25% faster than next minimum. As an extra criterion, we only considered LLJ event when the above criteria are satisfied in at least two consecutive soundings. These criteria were adapted from ones used to identify LLJ in Cabauw, Netherland, by Baas et al. (2009). This choice was based on the fact that LLJs in Cabauw and MRSP have similar depth and intensity. Soundings carried out during disturbed conditions that did not yield any resemblance with the thermodynamic structure used as reference were removed from the analysis. From 160 soundings, three were removed from daytime (21, 25, and 26 February) and five from nighttime (27 and 28 February and 11, 14, and 15 August) periods. During daytime the structure of lower atmosphere diverged from reference due to the rain associated synoptic-scale disturbance in the afternoon or the presence of very intense thermal inversion early in the morning. During nighttime, sea breeze early in the evening and cold fronts inhibited the formation of SI layer (see Figure 7 in section 4.1).

3.1.1. Performance Assessment of the Subjective Method

Objectively, the subjective method performance depends, to a large extent on how much the analyzed profiles differ from the reference ones, which in turn depends on how much the atmospheric conditions are

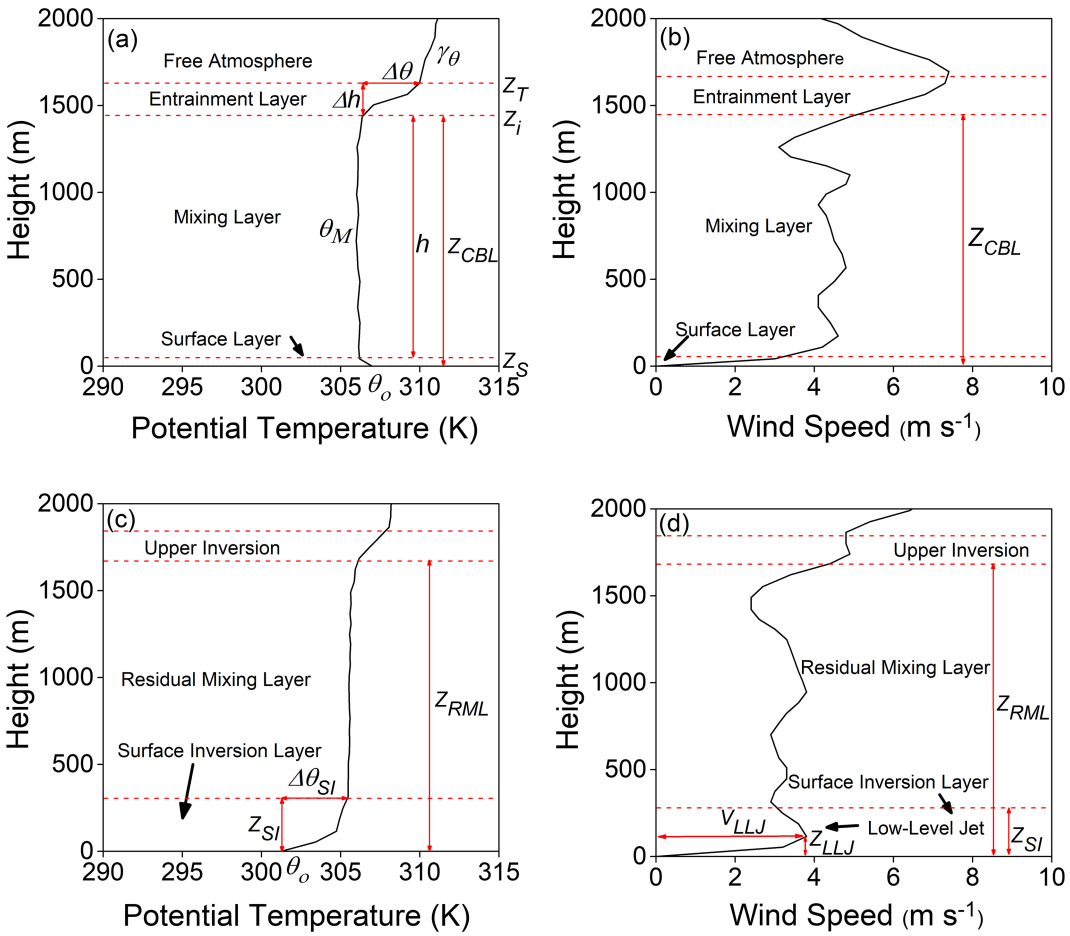

Figure 4. Soundings carried out on 8 and 9 August 2013, at (a, b) 1500 LT and (c, d) 2100 LT used as a reference of daytime and nighttime thermodynamic and dynamic PBL structures in the subjective method.

disturbed. Subjectively, the performance also relies on how familiar the person applying this method is with the local features of the climate. For these reasons, the subjective method is time consuming, difficult to apply to a large data set and suffer from two chronic problems: hard to reproduce and lack of traceability. One way to overcome these problems is to apply an objective method (Huang et al., 2017; Lee & De Wekker, 2016; Seidel et al., 2010; Zhang et al., 2014). Unfortunately, there is no objective method that yields all thermodynamic and dynamic PBL features detected by subjective method (Figure 4). Even if there was such method, it would be still facing a traceability problem due to the lack of a reference for performance testing. This later issue can only be answered from the observational point of view by combining traditional rawinsonde and remote sensing techniques. From the numerical modeling point view only high-resolution simulations of turbulence for both stable and convective regimes can provide the necessary reference data for a variety land cover and topography conditions.

A practical way to address this issue is comparing PBL properties that could be estimated by both objective and subjective methods. Daytime PBL heights estimated by the subjective method used here were compared to estimated values by three intensively used objective methods: air temperature gradient, air parcel and bulk-Richardson number (Ri_B) (Seibert et al., 2000; Zhang & Li, 2019). The PBL height in the air gradient method is estimated as the level where the vertical gradient of temperature becomes positive or equals 0 ($\partial T/\partial z \geq 0$). In the air parcel method, the PBL height is given by the level where an air parcel, raised adiabatically from the surface, crosses the potential-temperature vertical profile. In the Ri_B method, the PBL height is estimated as the level where the Ri_B reaches its critical value for the first time. In this study we used a critical value of 0.17 estimated according to the methodology described by Sorensen et al. (1996). It

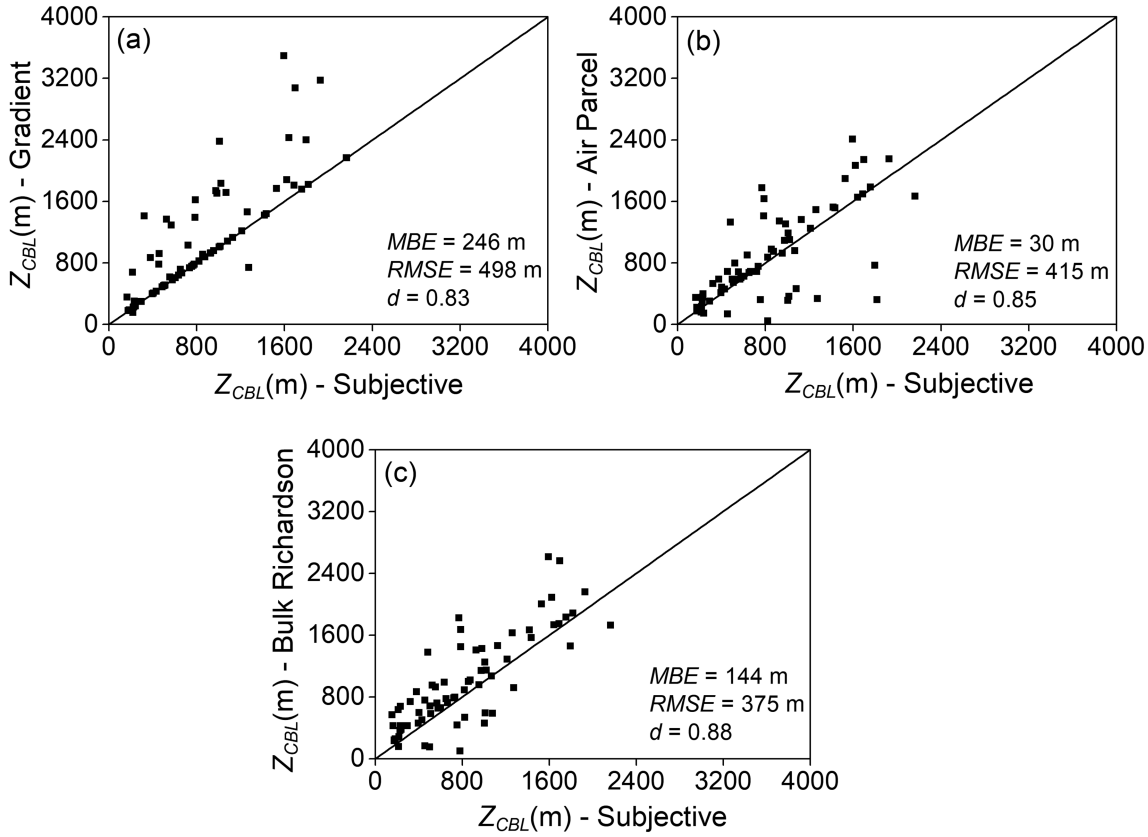

Figure 5. Dispersion diagrams of daytime PBL heights estimated by subjective method versus (a) air temperature gradient, (b) air parcel, and (c) bulk-Richardson number methods using rawinsondes carried out during MCITY BRAZIL Project field campaigns of February and August in 2013. In (c) critical Ri_B is 0.17.

corresponds to the minimum value of root-mean-square error (*RMSE*) of the UBL observed and estimated heights using different critical values of the Ri_B.

To objectively compare all methods, it was applied the following statistical parameters: mean bias error (*MBE*), *RMS*E, and the index of agreement (*d*). Positive *MBE* values indicate that subjective method underestimate objective method results and vice versa. The index of agreement, *d*, varies between 0 and 1 and indicates the level of fitness between "estimates" (subjective method) and "measurements" (objective method) (Willmott, 1981). Values of *d* close to 1 indicate a perfect performance of the estimates with respect to the measurements. As it can see in the Figure 5, the subjective method performs well, retrieving most of the PBL heights obtained by the objective methods. The best performance is presented when compared with Ri_B method, with $MBE = 144$ m, $RMSE = 375$ m, and $d = 0.88$. With $MBE = 246$ m, $RMSE = 498$ m, and $d = 0.83$ the subjective method does not perform so well when compared with gradient method. The subjective method performance can be categorized as intermediate with $MBE = 30$ m, $RMSE = 415$ m, and $d = 0.85$ when compared with air parcel method.

Taking into consideration the excellent performance displayed by subjective method with respect to these three objective methods it is plausible to assume that subjective method used here (section 3.1) yields comparable results for PBL height during daytime, indicating that this specific PBL property can be reproduced by the subjective method to an acceptable level of traceability given by the statistical parameters used here.

3.2. Objective Method

To estimate the top of the UBL based on regular soundings (twice a day), we will demonstrate the RML top height is a good indication of the CBL maximum daytime evolution (Figure 6a). This is necessary because in the case of São Paulo, as in most of the upper air stations in Brazil, rawinsondes are carried out at 0900 LT (1200 UTC) and 2100 LT (0000 UTC). At 0900 LT, the CBL is too shallow to be detected by the soundings with coarse resolution (data spacing 300 m) and in many days nonexistent. At 2100 LT, the SBL is also

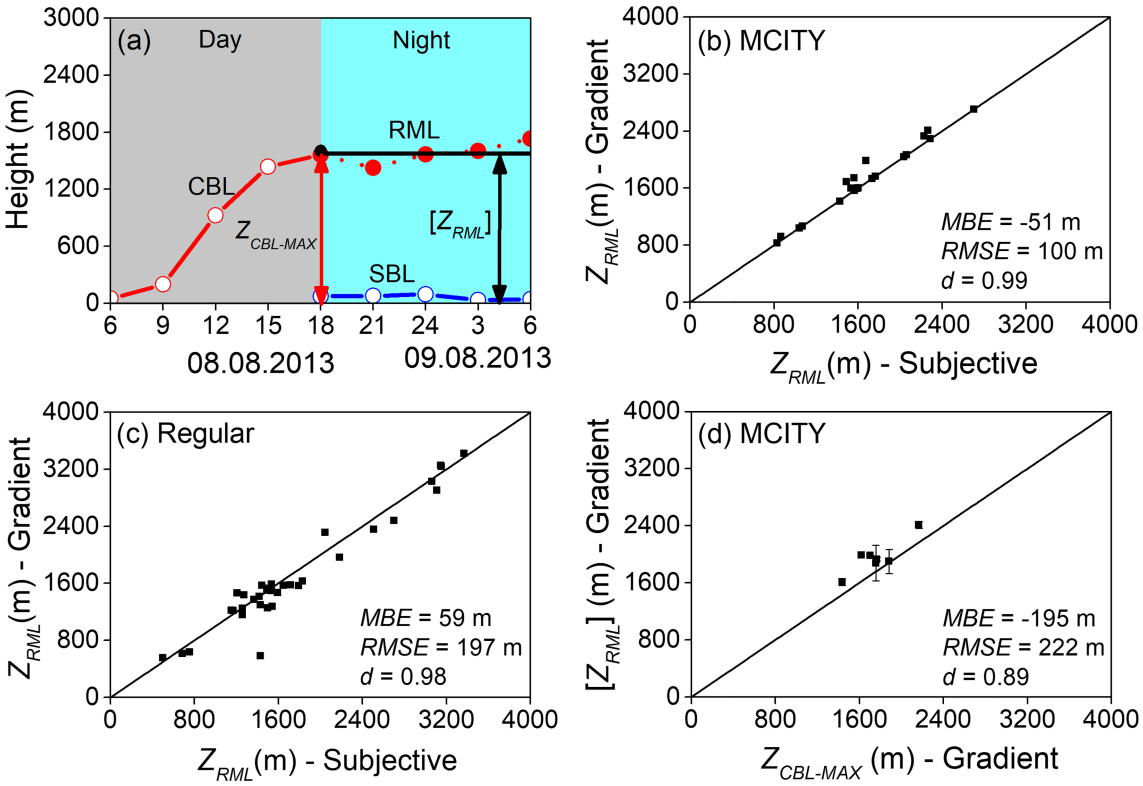

Figure 6. (a) Schematic representation of the maximum CBL height and mean RML top height. Dispersion diagrams of RML heights estimated by subjective and air temperature gradient methods for rawinsondes carried out (b) during MCITY BRAZIL Project field campaigns of February and August in 2013 and (c) June, July, and August of 2012. Dispersion diagram in (d) displays the comparison between mean RML top height (using air temperature gradient method) and previous maximum daytime UBL height (using air temperature gradient method) for rawinsondes carried out during the MCITY BRAZIL Project field campaigns of February and August in 2013. In (d), the vertical bars indicate statistical errors.

too shallow to be detected by the regular soundings (Figure 3b). Therefore, the only clear PBL feature that can be estimated from these coarse resolution soundings is the RML top.

To estimate the top of the RML, the objective method of the air temperature gradient (Seidel et al., 2010) was chosen. The performance of the air temperature gradient method was evaluated by comparing it with the subjective method in Figures 6b and 6c. Good agreement was obtained for the fine-resolution rawinsondes carried out during the two MCITY field campaigns in 2013 (Figure 6b). In this case, the *MBE*, *RMSE*, and *d* are −51 m, 100 m, and 0.99, respectively. A similar performance was obtained by regular coarse-resolution rawinsondes (Figure 6c). In this case the RML heights was also obtained by the subjective method using rawinsondes carried out at 2100 LT between June and August of 2012 by Valença (2013). The *MBE*, *RMSE*, and *d* are 59 m, 197 m, and 0.98, respectively.

To demonstrate that the RML top height can be used as an indication of the maximum daytime UBL height (as indicated in Figure 6a), we compared the maximum CBL height ($Z_{CBL-MAX}$) with the mean nighttime RML height ($[Z_{RML}]$), both obtained by the air temperature gradient method using rawinsondes carried out during the MCITY BRAZIL field campaigns in 2013. Figure 6d indicates that there is good agreement between $Z_{CBL-MAX}$ and $[Z_{RML}]$. The *MBE, RMSE* and *d* for these estimates are −195 m, 222 m, and 0.89, respectively, corroborating that RML top height can be used as a good indication of the UBL maximum daytime evolution. It is important to emphasize that small variation presented by the RML top height, as indicated by the small error bars displayed in five data points in Figure 6d (but visible only in two), does also contribute to make them a very good surrogate to UBL maximum daytime evolution, mainly when only one rawinsonde is available during nighttime as in the case of Brazil.

Taking into consideration the good performance of the air temperature gradient method, it was applied to the entire data set consisting of four years of data from September 2009 to August 2013. As an extra

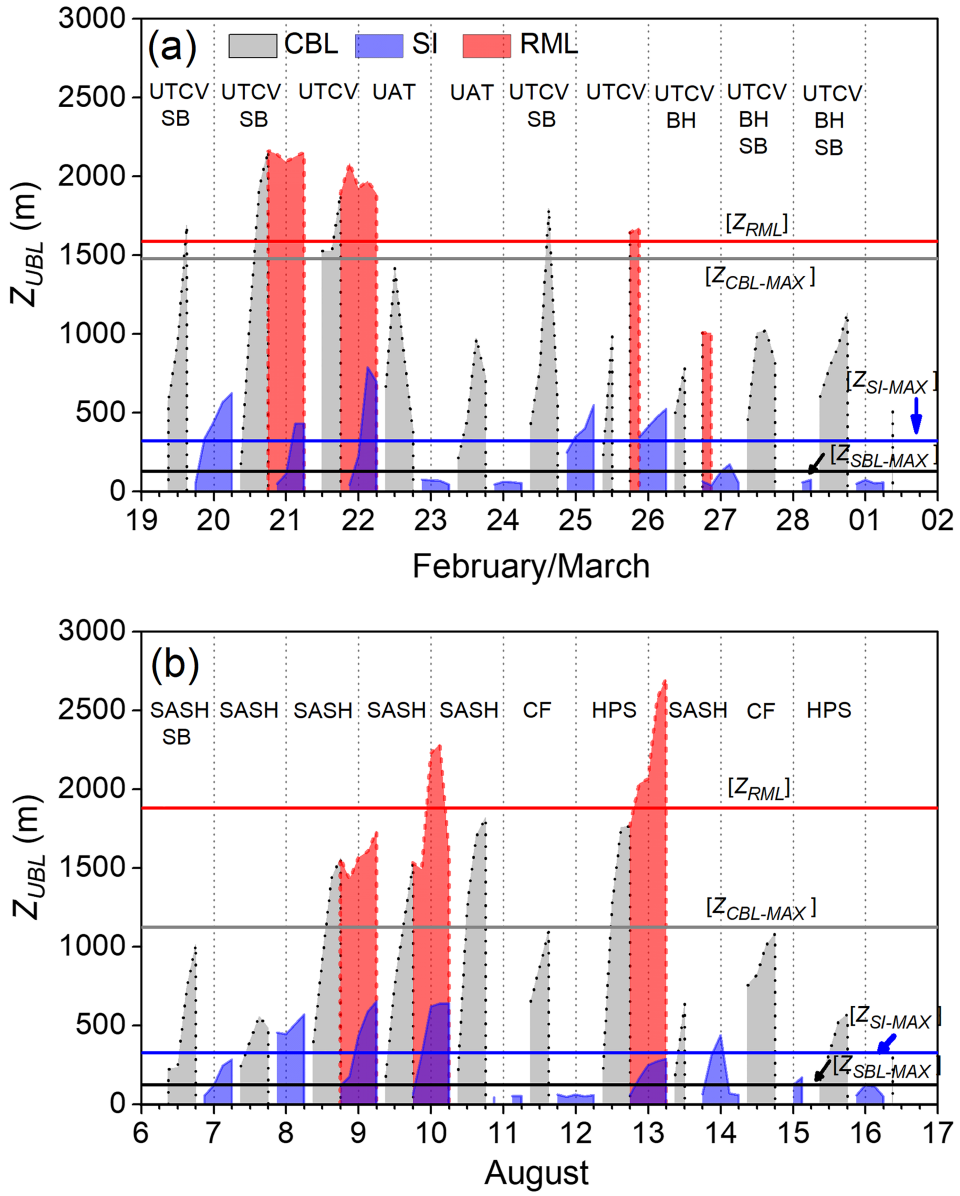

Figure 7. Diurnal evolution of the UBL and SI layer heights during the field campaigns. The horizontal gray, black, and blue lines indicate the mean values of the maximum heights of the CBL, SBL, and SI layer, respectively ($[Z_{CBL\text{-}MAX}]$, $[Z_{SBL\text{-}MAX}]$ and $[Z_{SI\text{-}MAX}]$). The horizontal red line indicates the mean height of the RML ($[Z_{RML}]$). The symbols correspond to the following synoptic disturbances: Upper Air Trough (UAT), Cold Front (CF), Bolivia High (BH), Upper Tropospheric Cyclonic Vortex (UTCV), Sea Breeze (SB), South Atlantic Subtropical High (SASH), and Post-Frontal High Pressure System (HPS).

condition, the RML top height was considered valid only when it was within 500 and 3,500 m. This condition was necessary to remove any misdetection caused by the SI layer. A total of 671 rawinsondes from 1,300 (51%) indicated a RML presence. This result will be discussed in the next section.

3.3. Empirical Method

In this work, the height of the SBL was estimated using an equilibrium expression derived by Zilitinkevich (1972). This expression was developed by the combination of parameters of the SI layer and is defined as

$$Z_{SBL} = \gamma_c (u_{*o} L / |f|)^{1/2}, \quad (1)$$

where u_{*o} is the friction velocity at the surface, L is the Obukhov length, f is the Coriolis parameter ($f = 0.000058\ s^{-1}$ for the latitude of São Paulo) and γ_c is the nondimensional parameter. In the literature, the

value of this empirical constant varies between 0.1 and 1 (Arya, 1981; Brost & Wyngaard, 1978; Garratt, 1982; Mahrt et al., 1982; Zilitinkevich, 1972). The present study uses $\gamma_c = 0.5$. This value was validated with high-resolution data from tethered balloon soundings carried out at a rural area located approximately 80 km west of the MRSP (Oliveira et al., 1998). The parameters u_{*o} and L were obtained from measurements made at IAG (Figure 1) (section 2.3.2).

It should be emphasized that expression (1) is widely used for practical applications (Seibert et al., 2000). Besides, there are evidences based on several different data sets (CASES99, Sodankylä, Cabauw, and SHEBA) and numerical results using LES modeling supporting the use of simple empirical expressions, similar to (1), to estimate SBL height (Steeneveld et al., 2007). Moreover, expression (1) was previously validated using fine resolution tethersonde data (5 m) gathered in industrial installation located at similar latitude, altitude, and climate conditions to the MRSP (Oliveira et al., 1998).

Friction velocity, vertical flux of buoyancy, $\overline{(\theta_V' w')}_0$, and Obukhov length are estimated using eddy covariance method as

$$u_{*0} = \left[\overline{(u'w')}_0^2 + \overline{(v'w')}_0^2\right]^{1/4} \tag{2}$$

$$L = {u_{*o}}^3 / \left[\frac{g}{\overline{\theta_v}}\overline{(\theta_V' w')}_0\right] \tag{3}$$

$$\overline{(\theta_V' w')}_0 = \overline{(\theta' w')}_0 + 0.61\ (\overline{\theta}/\overline{\rho})\overline{(\rho'_{H2O} w')}_0 \tag{4}$$

where ρ is air density, g is the acceleration due to gravity (9.81 m s^{-2}), θ is the potential temperature, and θ_v is the virtual potential temperature, $\overline{()}$ indicates 30-min mean and $(')$ respective statistical fluctuation given by $X' = X - \overline{X}$, for $X = u,\ v,\ w,\ \theta_v, \rho_{H2O}$.

4. UBL Properties

In this section, the main thermodynamic and dynamic characteristics of the UBL in the MRSP are described, considering vertical profiles of potential temperature, specific humidity, wind speed, and direction in the first 4,000 m of height of the soundings carried out in the ACM during 10 days in February representing a summer condition and 10 days in August of 2013 representing a winter condition (MCITY BRAZIL field campaigns).

4.1. Synoptic and Mesoscale Effects

Weather conditions have a significant effect on the development of the PBL (Guo et al., 2016; Quan et al., 2013). The time evolution of the UBL in the MRSP during the summer and winter campaigns of the MCITY BRAZIL Project are indicated in Figure 7. In these two periods the UBL evolution respond to the cloudiness pattern associated to the following synoptic and mesoscale systems: (a) Upper Air Trough, (b) Cold Front (de Jesus et al., 2016; Foss et al., 2017), (c) Bolivia High (Lenters & Cook, 1997), (d) Upper Tropospheric Cyclonic Vortex (Kousky & Gan, 1981; Mishra et al., 2001; Mishra et al., 2007), (e) Sea Breeze (Freitas et al., 2007; Oliveira et al., 2003; Ribeiro et al., 2018; Vemado & Pereira Filho, 2016), (f) Post-Frontal High-Pressure System (de Jesus et al., 2016; Foss et al., 2017), and (g) South Atlantic Subtropical High (Sun et al., 2017).

During the summer field campaign of February, cloudy conditions and rain accumulations are frequently associated with shortwave upper air trough west of São Paulo. As this shortwave moves east, the vorticity conservation requires horizontal divergence at high levels inducing upward movement and favoring cloud formation. This synoptic pattern was observed on 22 and 23 February, when the maximum UBL heights during daytime (1,419 and 975 m, respectively) were significantly lower than average ([$Z_{CBL\text{-}MAX}$], Figure 7a). On 26–28 February the daytime UBL evolution (789, 1,022, and 1,070 m, respectively) was also inhibited by the presence of cloudiness. In these cases, cloudiness was induced by high-level horizontal divergence produced by a combination of Bolivia high and upper tropospheric cyclonic vortex. On the other hand, during the summer field campaign clear sky conditions in the MRSP were associated to subsidence induced by an upper tropospheric cyclonic vortex. On 19–21, 24, and 25 February (Figure 7a), this vortex was positioned

north-east of the MRSP, inducing subsidence and favoring clear sky conditions. During these days, a more intense vertical development was observed in the UBL with maximum heights varying from 1,600 to 2,000 m (Figure 7a). This behavior indicates that the positive impact in the UBL growth caused by clear skies conditions overcompensates for the negative impact caused by subsidence in São Paulo during these days.

During the winter field campaign of August, the MRSP was dominated by a surface anticyclonic circulation associated with postfrontal high-pressure systems moving northeast and merging, progressively, with the semistationary South Atlantic subtropical high. Considered as a typical undisturbed condition, this synoptic pattern inhibits cloud formation in the MRSP resulting in the clear sky days observed on 8–10 and 12 August when the UBL height exceeded 1,500 m (Figure 7b). This pattern was momentarily disrupted by a cold front passage on 11 and 14 August (Figure 7b). In these cases, the maximum UBL depths (1,100 and 1,081 m, respectively) were smaller than the average ([$Z_{CBL\text{-}MAX}$], Figure 7b).

Sea breeze penetration in the MRSP occurs in the beginning of the afternoon and is characterized by a sharp decrease in air temperature and an increase in wind speed, cloudiness and relative humidity, and a shift in wind direction from northeast to southeast (Oliveira et al., 2003). According to Ribeiro et al. (2018), the sea breeze brings colder and moister air from the Atlantic Ocean, generating an internal boundary layer that disrupts the convective grown reducing the UBL height in São Paulo in most of the cases (19, 24, 27, and 28 February in Figure 7a and 6 August in Figure 7b). The apparent undisturbed UBL evolution observed on 20 February (Figure 7a) occurred because the sea breeze circulation was not strong enough.

During undisturbed nights in the summer (19–21, 24, and 25 February, Figure 7a) and winter (6–9 and 12 August, Figure 7b) of field campaigns the mean SI layer height was 376 ± 30 m, mean SBL height 74 ± 7 m, and mean RML height 1839 ± 55 m. During disturbed nights in both field campaign periods, the mean SI layer height was 79 ± 9 m, mean SBL height 83 ± 9 m, and RML was not present. Comparatively, undisturbed conditions (clear sky) are associated to strong surface cooling and light winds, as consequence the SBL are small and some cases inexistent, SI layer are deeper than SBL and the RML occurred in 60% of the nights. Disturbed conditions (cloudy) are associated to weak surface cooling and stronger winds, as consequence the SBL coincides with smaller SI layer. During both field campaigns a RML was observed in only one sounding (at 2100 LT on 26 February, Figure 7a). The deeper SI layer observed under undisturbed conditions occurs because the winds are lighter and radiative cooling is more important than turbulent cooling of the atmosphere near the surface.

4.2. Typical Undisturbed UBL

Figure 8 displays the time evolution of vertical profiles of potential temperature and wind speed in the first 3,000 m in summer and winter based on soundings carried out during daytime (0600 to 1800 LT) on 20 February and nighttime (1800 LT to 0600 LT) on 8 and 9 August 2013. They exemplified the UBL and LLJ characteristics estimated by the subjective method.

During daytime, the UBL in the MRSP is characterized by a ML in both summer and winter field campaigns. As indicated in Figure 8a, in the summer (20 February 2013) campaign, the turbulent mixing was strong enough to vertically homogenize the atmosphere. The 0600 LT profile (Figure 8a) shows that a SI layer formed during the previous night (9 to 20 February) that reached a maximum height of 623 m. At 0900 LT, the lower portion of the SI layer was completely replaced by a CBL of 176 m. The UBL reached 2,166 m on 20 February at 1800 LT.

During nighttime, the SI layer is indicated in the winter soundings carried out from 8 August at 1800 LT to 9 August at 0600 LT (Figure 8c). There, the SI layer depth grew from 115 m with $\theta_{SI}/Z_{SI} = 7.8$ K km^{-1} at 1800 LT to 652 m with $\theta_{SI}/Z_{SI} = 20$ K km^{-1} at 0600 LT. The UBL height given by the empirical expression (1) varied from 75 m at 1800 LT to 44 m at 0600 LT. In that case, the SI layer cannot be used as an indication of the UBL height. Above the SI layer, a RML was observed at heights between 1,400 and 1,800 m (within the parallel dashed red lines in Figure 8c).

An LLJ with an intensity of 5.8 m s^{-1} and direction from the north was present at 240 m in the MRSP during the night of 8 and 9 August 2013 (Figure 8d). This LLJ was present in the sounding of 0000 LT and reached a maximum intensity of 11 m s^{-1} and height of 414 m at 0600 LT (Figure 8d). At the maximum intensity core, the wind direction was from the north.

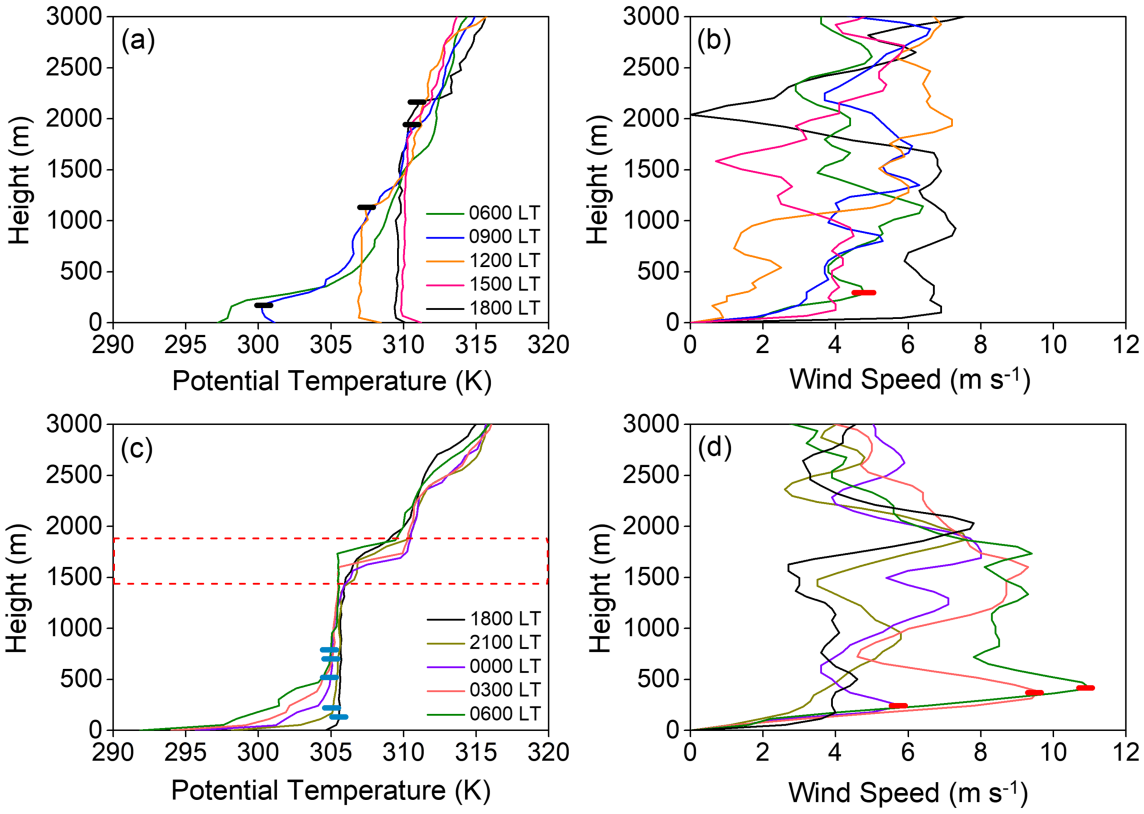

Figure 8. Vertical profiles of potential temperature and wind speed observed during daytime (0600–1800 LT) on (a, b) 20 February 2013 (summer) and during nighttime (1800–0600 LT) on (c, d) 8–9 August 2013 (winter) in the MRSP. The top of the convective UBL height is indicated by the heavy dark horizontal lines in (a). The top of the SI layer height is indicated by heavy blue horizontal lines in (c). The dashed red horizontal lines indicate the upper air temperature inversion and the top of the RML in (c). The LLJ height is indicated by horizontal heavy red line in (b) and (d).

4.3. Seasonal Variation

4.3.1. Daytime Features

The SL thickness corresponds to 10% and 12% of the UBL height during the summer and winter field campaigns, respectively, varying from 33 to 152 m in February and from 27 to 126 m in August (Figure 9a). A ML is present in most of the soundings carried out at 0900 LT, indicating that the SI layer formed during the previous night is completely destroyed by thermal convection in the MRSP before 0900 LT. It is also observed that the ML grows systematically until the end of the day, which is in general at approximately 1800 LT. The thickness of the ML varies from 110 m to 2,097 m in the field campaign of February and from 109 to 1,694 m in the field campaign of August, corresponding to 90% and 88% of the UBL height, respectively (Figure 9b).

The entrainment layer varies between 47 and 352 m in the field campaign of February and between 23 and 385 m in August and corresponds to 16% and 17% of the UBL height, respectively (Figure 9c). The thermal inversion strength in the entrainment layer varies from 2.7 to 41.4 K km^{-1} in the field campaign of February and from 3.4 to 56.4 K km^{-1} in the field campaign of August, indicating that entrainment layer is less stable during summer than during winter (Figure 9d).

The stability of the free atmosphere immediately above the UBL varies from 2.1 to 5.5 K km^{-1} during the February campaign and 1.5 to 8 K km^{-1} in the August campaign. The free atmosphere immediately above the UBL is frequently less stable during summer compared to winter, with mean values of 3.3 ± 0.1 K km^{-1} in February and 3.9 ± 0.2 K km^{-1} in August (Figure 9e).

4.3.2. Nighttime Features

During nighttime, the maximum height of the SI layer varied, ranging on average from 322 ± 80 m in February to 326 ± 74 m in the August campaign. In many studies, the top of the UBL during nighttime

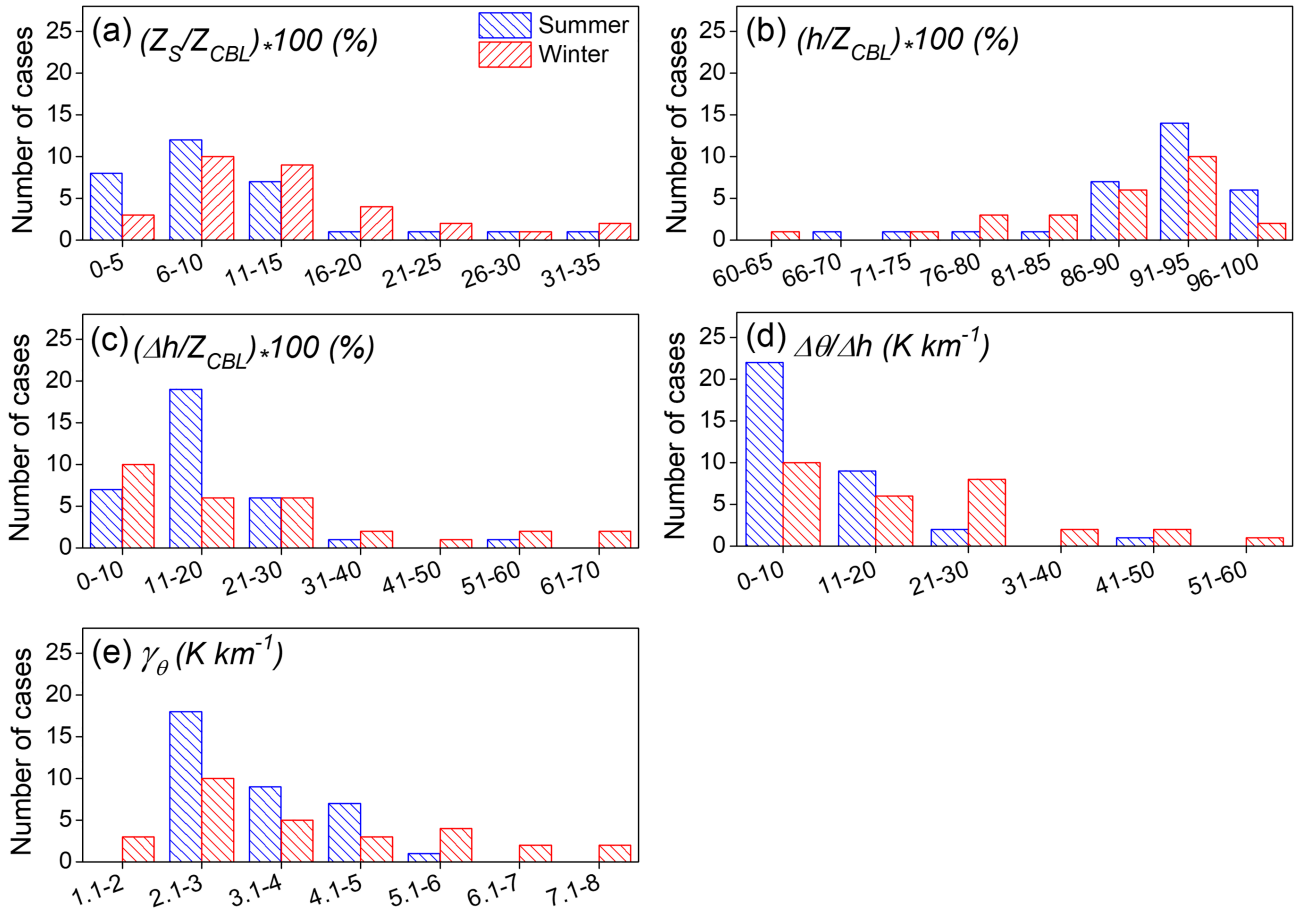

Figure 9. Daytime properties of the UBL in MRSP during the summer and winter campaigns based on the subjective method. Frequency distribution of the fraction of UBL occupied by the (a) SL, (b) ML, and (c) entrainment layer. Frequency distribution of the (d) upper inversion strength and (e) vertical gradient of potential temperature in the free atmosphere adjacent to the UBL. The results are shown relative to the CBL height in (a)–(c). Number of cases corresponds to number of soundings.

was indicated by SI layer top (Coulter, 1990; Pournazeri et al., 2012; Seidel et al., 2010; Wang & Wang, 2016; Yu, 1978). For São Paulo, sea breeze circulation significantly alters the daytime evolution of the UBL. The sea breeze fronts propagate from southeast to northwest, generating abrupt drops in temperature followed by abrupt increases in humidity (Oliveira et al., 2003). These changes occur during the afternoon, and in many cases, the associated surface cooling generated a SI layer extending to the top of the sea breeze layer, a condition that persists through the night (Ribeiro et al., 2018). The changes caused by sea breeze mask the nocturnal evolution of the SI layer associated with turbulence, making it difficult to estimate the UBL from rawinsondes during the night in São Paulo.

Figure 10 shows the frequency distribution of the SI layer height estimated by the subjective method (section 3.1) and the SBL estimated by the empirical method (section 3.3). The height of the SBL remained on average 180 m below the height of the SI layer in February and 174 m in August. These differences may occur because the SBL depth decreases as the turbulence intensity decreases due to the intensification of thermal stability caused by surface radiative cooling (Garratt, 1994).

A very well defined RML was observed during nighttime soundings, generally after 1800 LT, on approximately 35% of the nights with soundings and RML top height varied from 800 m to 2,300 m in the February campaign and between 1,400 and 2,700 m in August (Figure 10g).

The LLJ was observed in 80% of the nights with soundings (16 nights, 9 in summer, and 7 in winter), was located between 95 and 962 m (Figure 10c), and had a speed varying from 2.7 to 14 m s^{-1} (Figure 10d). The north, northeast, east and southeast wind direction components prevailed in most of the observed

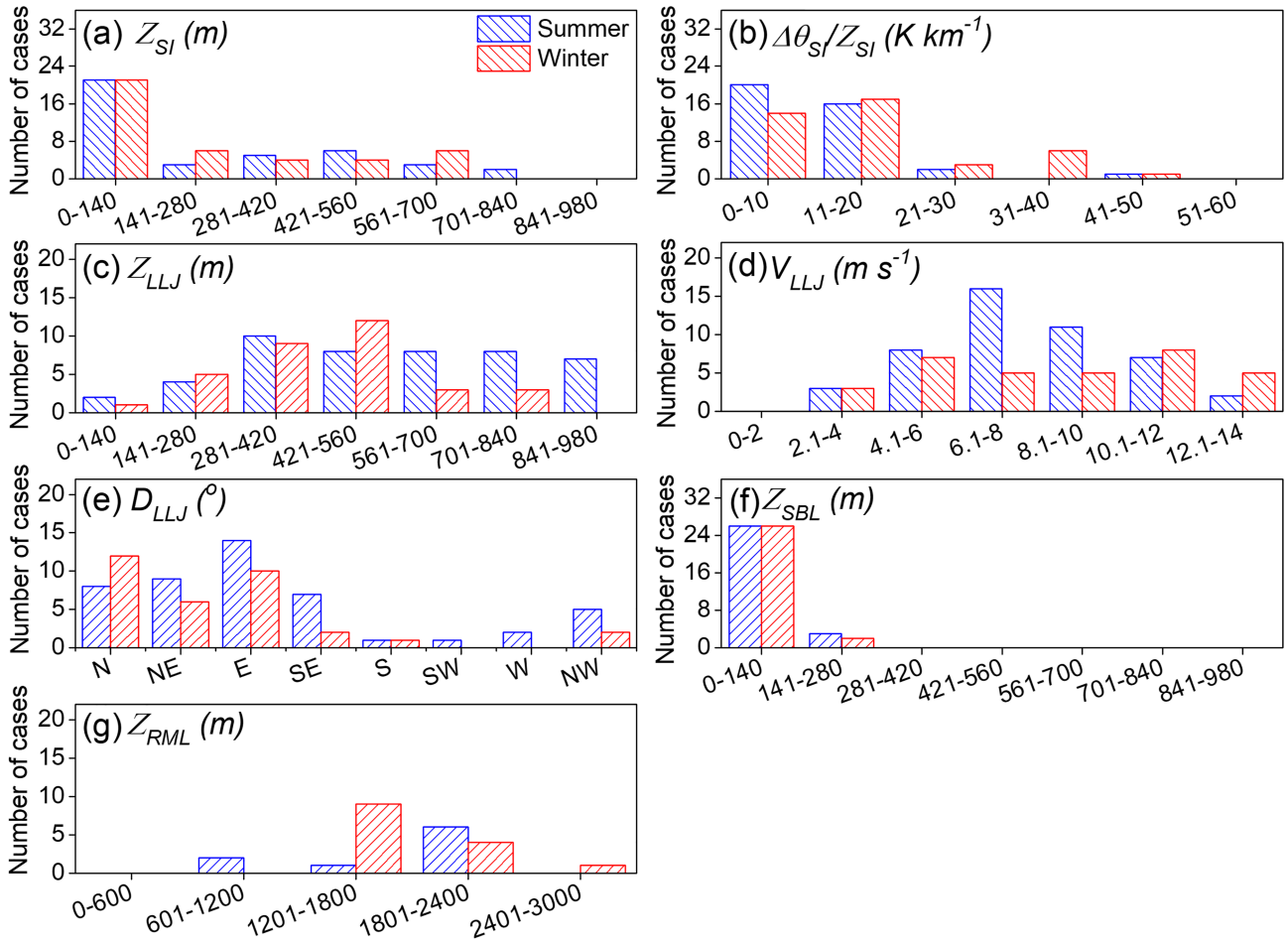

Figure 10. Nighttime properties of the UBL in the MRSP during the summer and winter campaigns based on the subjective and empirical methods. Histograms of (a) SI Layer height, (b) strength of the SI layer, (c) LLJ height, (d) LLJ wind speed, (e) LLJ wind direction, (f) SBL height, and (g) RML height. Number of cases corresponds to number of soundings.

LLJ (Figure 10e). Although there is evidence that wind speed during nighttime oscillates inertially in the presence of LLJ, the origins of this phenomena in the MRSP remain unclear and will be addressed in future work.

4.3.3. Mean Diurnal Evolution

Figure 11 displays the diurnal evolution of the averaged UBL and SI layer heights during the summer and winter field campaigns of 2013 in the MRSP and the buoyancy flux estimated in the IAG by expression (4). The UBL height in summer was larger than in winter because the daily values of mean buoyancy flux (Figures 11c and 11d) in the summer (4.7 ± 0.6 MJ m^{-2} day^{-1}) was 30% larger than in the winter (3.3 ± 0.5 MJ m^{-2} day^{-1}), and as a consequence, the thermal production of turbulent kinetic energy (TKE). Another important factor that contributed to the observed pattern is that the thermal stratification in the free atmosphere immediately above the top of the UBL was weaker during summer (Figure 9e).

In both periods investigated here, the maximum top of the UBL was observed at 1800 LT. On average, the maximum UBL height was 1476 ± 149 m in the February campaign and 1122 ± 168 m in the August campaign (Figures 11a and 11b). The SI layer showed a similar but less pronounced seasonal variation that reached a maximum height (and strength) of 322 ± 80 m (18 ± 3 K km^{-1}) in February and 326 ± 74 m (22 ± 4 K km^{-1}) in August (Figures 11a and 11b). The SBL showed a similar behavior in both experiments, reaching a maximum height between 1800 and 2100 LT, on average, from 126 ± 13 m in February and 122 ± 10 m in August. This was due to a higher mechanical production of TKE in the early evening associated with the passage of the sea breeze on many occasions (Figures 11a and 11b).

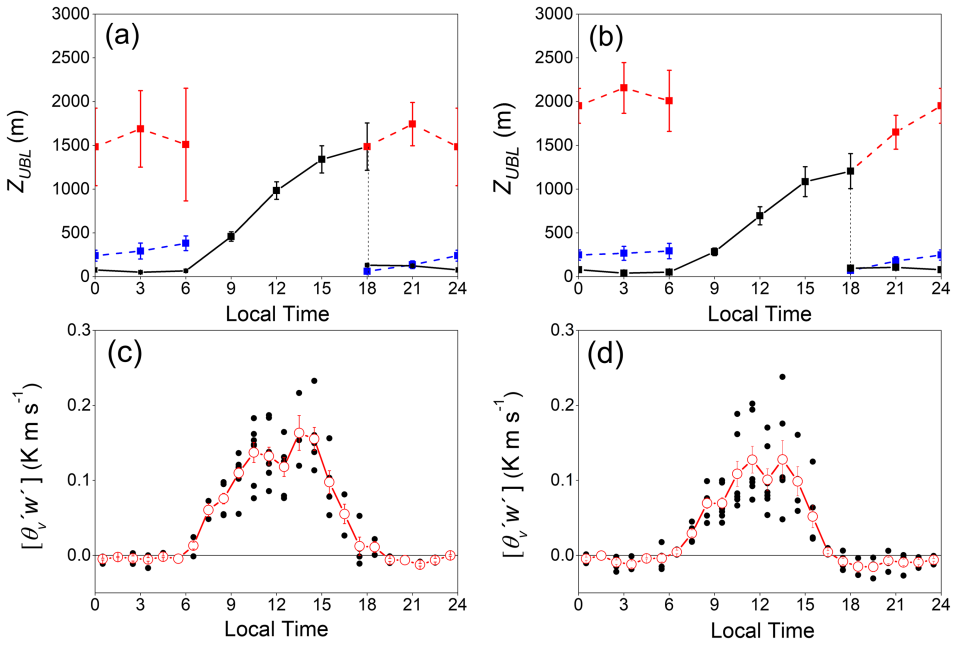

Figure 11. Diurnal evolution of the UBL and SI layer heights and buoyancy flux averages during 10 days in the (a–c) summer and (b–d) winter field campaigns. The vertical bars indicate statistical error. The black, blue and dashed red lines in (a) and (b) indicate the heights of the UBL, SI layer, and RML, respectively. The black solid circles in (c) and (d) indicate hourly values of buoyancy flux.

On average, the RML top height (indicated by the red dashed lines in Figures 11a and 11b) shows a seasonal pattern consistent with UBL ones, with values varying between 800 and 2,300 m in February and 1,400 and 2,700 m in August. Due to the number of nights with RML in both periods (7 of 20 nights), on average, the RML top height was systematically higher than the UBL height, mainly during the winter campaign. In addition to the spatial representativeness factor, the differences in the UBL and RML top heights may have been related to the variations in the trajectories described by the soundings.

Observations carried out by Nair et al. (2004) using a Doppler sodar on 27 July 1999, indicated that during nighttime the SI layer oscillate around 233 m between 0000 and 0800 LT and around 366 m between 1800 and 2400 LT. These are comparable with values obtained in August campaign (274 ± 42 m between 0000 and 0600 LT and 198 ± 36 m between 1800 and 2400 LT). During daytime on 27 July, the PBL height reached 1600 m at 1100 LT. This value is larger than 695 ± 103 m observed at 1200 LT in August campaign. The observations using lidar by Landulfo et al. (2010) in August of 2007 indicated daytime maximum heights varying between 1,100 and 2,800 m and mean value around 1,700 m, what is larger than mean maximum heights of 1122 ± 168 m observed in the August campaign.

4.3.4. Monthly and Interannual Variation

In this section, a climatological characterization of the maximum UBL top height in the MRSP is performed based on rawinsondes carried out daily at 2100 LT, from September 2009 to August 2013 and the air temperature gradient method described in section 3.2. As demonstrated in the previous section 3.2 the RML top height is a good indication ($d = 0.89$) of the CBL maximum daytime evolution (see Figure 6a).

Figure 12a shows the seasonal variations in the monthly average UBL height in the MRSP. The UBL height varied between 1,000 and 1,700 m. The largest value was observed in May (1632 ± 96 m), and the smallest was observed in September (1061 ± 77 m). During summer months (December–February) the number of RML detection was small because the local atmosphere was more disturbed as consequence of convective activity in the MRSP. The UBLs detected during the MCITY field campaigns in 2013 were systematically deeper than those detected by the regular soundings. A reduction in the cloudiness may explain this behavior since during the field campaign periods the MRSP was drier than normal (Figure 3b). During spring months the intensification of sea breeze circulation reduces the UBL height in the MRSP. This effect was observed also during the field campaigns (section 4.1). The passage of sea breeze front disrupts the UBL evolution in the afternoon (Ribeiro et al., 2018). This effect is stronger in the spring because during this period of the year the ocean-land

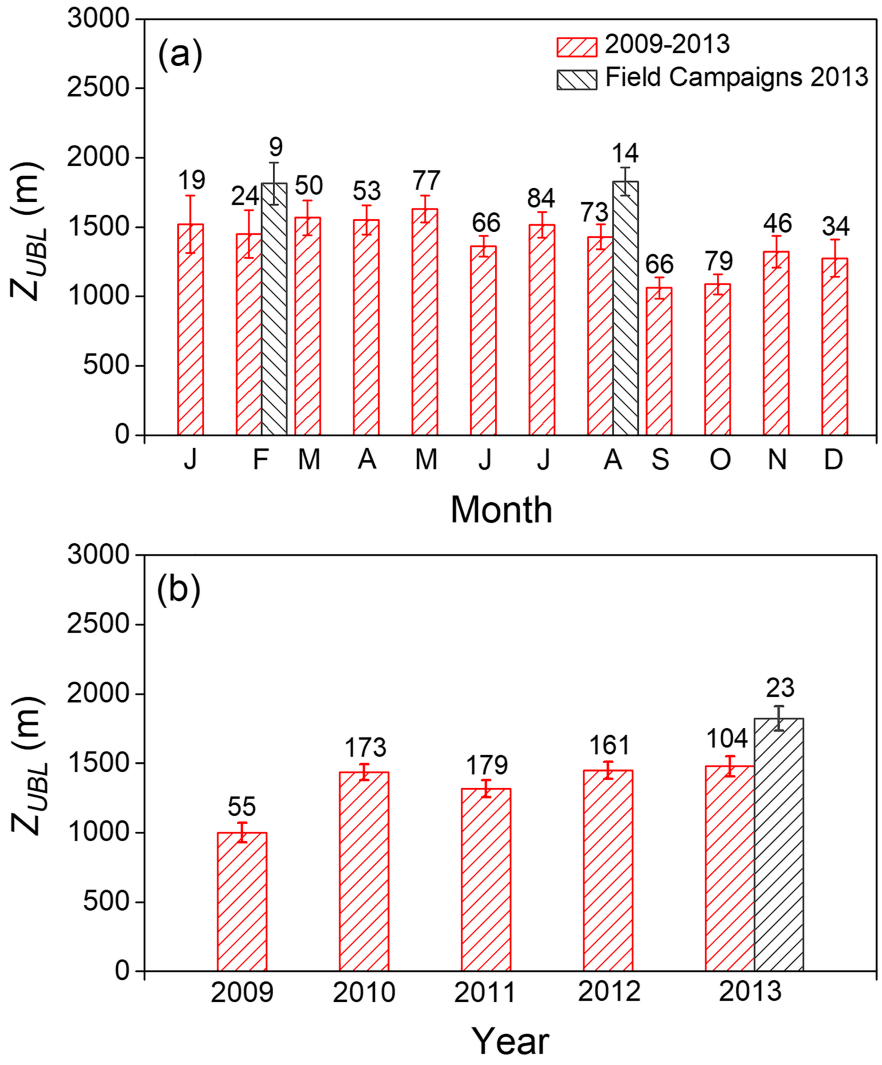

Figure 12. Seasonal and interannual variations in the monthly averaged UBL height in the MRSP. The statistical errors are indicated by the vertical bars. The numbers indicate the total number of days with RML.

thermal contrast is larger as consequence of the oceanic thermal inertial. Similar sea breeze effect has been found in the annual variability of PBL height estimated using wind profiler measurements carried out during one year (2008) in the California's Central Valley Observations (35–39°N) by Bianco et al. (2011).

The interannual variations between 2009 and 2013 did not show a clear pattern; the smallest UBL occurred in 2009 (999 ± 70 m), and the largest occurred in 2013 (1,478 ± 72 m) (Figure 12b). Since the UBL height is smaller during spring and beginning of summer months, the minimum UBL height observed in 2009 is because rawinsondes were available only from September 2009. A similar effect may explain the maximum UBL height observed in 2013. The rawinsondes data used in this year were carried only until 16 August, corresponding to the period when UBL is higher (January–August). Therefore, taking into consideration the representativeness problem one may conclude that between 2009 and 2013 there was not significant interannual variability in the UBL maximum daytime height in the MRSP.

5. Summary and Concluding Remarks

The vertical structure of the UBL in the MRSP was investigated in this work using rawinsondes carried out every three hours for two 10-day field campaigns of the MCITY BRAZIL Project in February and August 2013. This characterization was complemented using rawinsondes carried out regularly twice a day during four years, from 1 September 2009 to 16 August 2013.

The time evolution of the UBL in the MRSP during the summer and winter field campaigns responded to the cloudiness pattern associated to disturbances caused by synoptic and mesoscale systems. In general, these disturbances increase cloudiness, reducing surface solar heating and thermal production of TKE. Under these conditions, the daytime UBL is partially or totally maintained by mechanical production of TKE, and its depth is smaller than in clear-sky days. During nighttime, clouds reduce the surface cooling and the intensity of SI layer. The small thermal stratification combined with more strong winds favors the formation of deeper SBL.

During daytime, the UBL showed a maximum height reaching 1476 ± 149 m in the summer campaign of February and 1122 ± 168 m in the winter campaign of August of 2013. Those differences were related to seasonal variations in the (a) surface buoyancy flux, which was 30% larger in the summer (4.7 ± 0.6 MJ m^{-2} day^{-1}) and (b) thermal stratification of the free atmosphere, which was 15% smaller in the summer (3.3 ± 0.1 K km^{-1}). In both seasons water vapor flux did not contribute significantly to buoyancy flux and consequently to the UBL evolution in the MRSP as expected for urban areas. During nighttime, the maximum top height of the SI layer varied, on average, from 322 ± 80 m in February to 326 ± 74 m in August. In both experiments, the maximum height of the SBL reached 126 ± 13 m in February and 122 ± 10 m in August.

During daytime, a SL was observed in 82 % of the rawinsondes, with heights varying between 33 and 152 m in February and between 27 and 126 m in August that corresponded to 10% and 12% of the height of the convective UBL in both periods. The ML depth varied between 110 and 2,097 m in the field campaign of February and between 109 and 1,694 m in the field campaign of August. The entrainment layer, varied between 47 and 352 m in the field campaign of February and between 23 and 385 m in August.

During the night, the SI layer top height varied from 42 to 784 m in February and from 45 to 652 m in the August field campaign. It was systematically deeper than the SBL, which varied from 20 to 171 m in February and from 11 to 173 m in the August field campaign. A very well defined RML was observed generally after 1800 LT on approximately 35% of the nights in both field campaigns, varying from 800 to 2,300 m in the February campaign and from 1,400 to 2,700 m in August. The LLJ was observed in 80% of the field campaign nights, with intensities varying from 2.7 to 14 m s^{-1} and heights between 95 and 962 m. Although there is evidence of counterclockwise inertial oscillation in the LLJ observed in the MRSP, the origin of this phenomenon remains unclear and will be addressed in future work.

A comparative analysis between rawinsondes carried out at nighttime in the field campaigns in 2013 and at 2100 LT regularly from June to August of 2012 indicates that the air temperature gradient method is well suited to estimate the RML top height and that RML height is a good surrogate for the maximum daytime value of the UBL height in previous day. The seasonal variations in the monthly average maximum UBL height, based on application of the air temperature gradient method for rawinsondes carried out regularly in São Paulo at 2100 LT from September 2009 to August 2013, indicated a maximum of 1632 ± 96 m in May and a minimum of 1,061 ± 77 m in September. The seasonal variation of UBL, summer maximum and winter minimum, yielded from finer temporal and vertical resolution carried out during the MCITY BRAZIL Project in 2013 was not confirmed by the 4-year coarser resolution rawinsonde. Intensification of sea breeze circulation during spring is a plausible explanation for the observed minimum in the monthly averaged UBL height in September. No tendency was identified in the UBL height during 4 years (2009–2013) analyzed in this work, indicating that UBL in São Paulo does not seems to respond, as observed in other higher latitudes regions, to the current positive trend attributed to global climate changes.

The impact of climate change effects predicted by the Intergovernmental Panel on Climate Change scenarios indicated that Brazilian urban populations are likely to become more exposed to the adverse urban effects such as significant reduction on precipitation and augment in temperature (Batista et al., 2016; Lyra et al., 2018). On the other hand, long-term variation of PBL height carried out in Europe, China, and Japan (Guo et al., 2019; Zhang et al., 2013; Zhang & Li, 2019) indicated that there is an overall tendency to increase the PBL height as a response to the global warming, mainly increase in the surface temperature and reduction in the relative humidity. However, it is still not possible to infer what would be the impact of the Intergovernmental Panel on Climate Change scenarios on the PBL heights over urban areas. In this sense, the observational characterization of the UBL in São Paulo, even using only 4-year-long climatology, is the first one based on observational results about UBL in the subtropical region.

It is important to emphasize the results displayed here are the first analysis based on rawinsondes carried out in the MRSP. Since we demonstrated that the RML height, estimated by the air temperature gradient method using rawinsondes carried out regularly, is a good surrogate for the maximum daytime value of the UBL height, this objective method can be applied to estimate the PBL height for soundings carried out at 2100 LT in the entire network, allowing a long term spatial characterization of the PBL in Brazil.

Finally, despite the recent progress in the application of remote sensing systems to characterize PBL properties, it will take time and resources to disseminate them worldwide as rawinsonde network. Therefore, the use of rawinsonde data to estimate PBL properties will continue to be an important issue requiring attention for the research community, mainly to develop objective methods to detect a more complete set of PBL properties. The performance analyses carried out here indicated the subjective method yields comparable results for PBL height during daytime to an acceptable level of traceability. This assumption cannot be extrapolated for the other PBL properties because the lack of objective methods; however, it can be progressively assured ever since other PBL properties are estimated by the subjective method are objectively tested as the height of PBL.

Acknowledgments
This research was sponsored by the Brazilian Research Foundations: FAPESP (2011/50178-5), FAPERJ (E26/111.620/2011 and E-26/103.407/2012), CNPq (309079/2013-6,305357/2012-3 and 462734/2014-5), and CAPES (CAPES Financial Code 001). The first author acknowledges the scholarship provided by CNPq. Special thanks to Dayana Yordy Sánchez for help with the synoptic description. We would like to thank the Brazilian Air Force, especially Brigadier Luiz Cláudio Ribeiro da Silva, Colonel César Augusto Borges Tuna, Lieutenant Colonel Bernardino Simões Neto, Air Force Meteorologists Sergeant Luiz de Oliveira Hirt, and Major Milton Osamu Ojumura. This manuscript complies with FAIR DATA standards. Data are available in the data repository "Mendeley Data" entitled: "Urban Boundary Layer at Tropical Cities."

References

Alvares, C. A., Stape, J. L., Sentelhas, P. C., De Moraes Gonçalves, J. L., & Sparovek, G. (2014). Köppen's climate classification map for Brazil. *Meteorologische Zeitschrift*, *22*(6), 711–728. https://doi.org/10.1127/0941-2948/2013/0507

Arya, S. P. S. (1981). Parameterizing the height of the stable atmospheric boundary layer. *Journal of Applied Meteorology*, *20*, 1192–1202. https://doi.org/10.1175/1520-0450(1981)020<1192:pthots>2.0.co;2

Aubinet, M., Vesala, T., & Papale, D. (2012). *Eddy covariance: A practical guide to measurement and data analysis. Methods of Measuring Environmental Parameters.* Dordrecht Heidelberg London New York: Springer.

Baas, P., Bosveld, F. C., Baltink, H. K., & Holtslag, A. A. M. (2009). A climatology of nocturnal low-level jets at Cabauw. *Journal of Applied Meteorology and Climatology*, *48*, 1627–1642. https://doi.org/10.1175/2009JAMC1965.1

Banks, R. F., Tiana-Alsina, J., Rocadenbosch, F., & Baldasano, J. M. (2015). Performance evaluation of the boundary-layer height from lidar and the Weather Research and Forecasting Model at an urban coastal site in the north-east Iberian Peninsula. *Boundary-Layer Meteorology*, *157*(2), 265–292. https://doi.org/10.1007/s10546-015-0056-2

Barlow, J. F. (2014). Progress in observing and modelling the urban boundary layer. *Urban Climate*, *10*, 216–240. https://doi.org/10.1016/j.uclim.2014.03.011

Barlow, J. F., Halios, C. H., Lane, S. E., & Wood, C. R. (2015). Observations of urban boundary layer structure during a strong urban heat island event. *Environmental Fluid Mechanics*, *15*(2), 373–398. https://doi.org/10.1007/s10652-014-9335-6

Basha, G., & Ratnam, M. V. (2009). Identification of atmospheric boundary layer height over a tropical station using high-resolution radiosonde refractivity profiles: Comparison with GPS radio occultation measurements. *Journal of Geophysical Research Atmospheres*, *114*, D16101. https://doi.org/10.1029/2008JD011692

Batista, R. J. R., Gonçalves, F. L. T., & da Rocha, R. P. (2016). Present climate and future projections of the thermal comfort index for the metropolitan region of São Paulo, Brazil. *Climatic Change*, *137*(3–4), 439–454. https://doi.org/10.1007/s10584-016-1690-5

Beyrich, F. (1997). Mixing height estimation from sodar data. *Atmospheric Environment*, *31(23)*, 3941–3953. https://doi.org/10.1016/S1352-2310(97)00231-8

Bianco, L., Djalalova, I. V., King, C. W., & Wilczak, J. M. (2011). Diurnal evolution and annual variability of boundary-layer height and its correlation to other meteorological variables in California's Central Valley. *Boundary-Layer Meteorology*, *140*(3), 491–511. https://doi.org/10.1007/s10546-011-9622-4

Bornstein, R. D. (1987). *Mean diurnal circulation and thermodynamic evolution of urban boundary layer* (pp. 53–94). Boston, MA: American Meteorological Society.

Brost, R. A., & Wyngaard, J. C. (1978). A model study of the stably stratified planetary boundary layer. *Journal of Atmospheric Sciences*, *8*, 1427–1440.

Compton, J. C., Delgado, R., Berkoff, T. A., & Hoff, R. M. (2013). Determination of planetary boundary layer height on short spatial and temporal scales: A demonstration of the Covariance Wavelet Transform in ground-based wind profiler and lidar measurements. *Journal of Atmospheric and Oceanic Technology*, *30*, 1566–1575. https://doi.org/10.1175/JTECH-D-12-00116.1

Coulter, R. L. (1990). A case study of turbulence in the stable nocturnal boundary layer. *Boundary-Layer Meteorology*, *52*, 75–91. https://doi.org/10.1007/BF00123179

Dang, R., Yang, Y., Hu, X. M., Wang, Z., & Zhang, S. (2019). A review of techniques for diagnosing the atmospheric boundary layer height (ABLH) using aerosol lidar data. *Remote Sensing*, *11*. https://doi.org/10.3390/rs11131590

de Jesus, E. M., Rocha, R. P., Reboita, M. S., Llopart, M., Dutra, L. M. M., & Remedio, A. R. C. (2016). Contribution of cold fronts to seasonal rainfall in simulations over the southern la Plata Basin. *Climate Research*, *68*, 243–255. https://doi.org/10.3354/cr01358

Emeis, S., Münkel, C., Vogt, S., Müller, W. J., & Schäfer, K. (2004). Atmospheric boundary-layer structure from simultaneous SODAR, RASS, and ceilometer measurements. *Atmospheric Environment*, *38*, 273–286. https://doi.org/10.1016/j.atmosenv.2003.09.054

Feng, X., Wu, B., & Yan, N. (2015). A method for deriving the boundary layer mixing height from MODIS atmospheric profile data. *Atmosphere*, *6*, 1346–1361. https://doi.org/10.3390/atmos6091346

Fortuniak, K., Pawlak, W., & Siedlecki, M. (2013). Integral turbulence statistics over a central European city centre. *Boundary-Layer Meteorology*, *146*(2), 257–276. https://doi.org/10.1007/s10546-012-9762-1

Foss, M., Chou, S. C., & Seluchi, M. E. (2017). Interaction of cold fronts with the Brazilian Plateau: A climatological analysis. *International Journal of Climatology*, *37*, 3644–3659. https://doi.org/10.1002/joc.4945

Freitas, E. D., Rozoff, C. M., Cotton, W. R., & Silva Dias, P. L. (2007). Interactions of an urban heat island and sea-breeze circulations during winter over the metropolitan area of São Paulo, Brazil. *Boundary-Layer Meteorology*, *122*, 43–65. https://doi.org/10.1007/s10546-006-9091-3

Garratt, J. R. (1982). Observations in the nocturnal boundary layer. *Boundary-Layer Meteorology*, *22*, 21–48.
Garratt, J. R. (1994). *The atmospheric boundary layer*. Cambridge: Cambridge University Press.
Garreaud, R., & Wallace, J. M. (1998). Summertime incursions of midlatitude air into subtropical and tropical South America. *Monthly Weather Review*, *126*(10), 2713–2733. https://doi.org/10.1175/1520-0493(1998)126<2713:SIOMAI>2.0.CO;2
Guo, J., Li, Y., Cohen, J. B., Li, J., Chen, D., Xu, H., et al. (2019). Shift in the temporal trend of boundary layer height in China using long-term (1979–2016) radiosonde data. *Geophysical Research Letters*, *46*, 6080–6089. https://doi.org/10.1029/2019GL082666
Guo, J., Miao, Y., Zhang, Y., Liu, H., Li, Z., Zhang, W., et al. (2016). The climatology of planetary boundary layer height in China derived from radiosonde and reanalysis data. *Atmospheric Chemistry and Physics*, *16*, 13,309–13,319. https://doi.org/10.5194/acp-16-13309-2016
Hennemuth, B., & Lammert, A. (2006). Determination of the atmospheric boundary layer height from radiosonde and lidar backscatter. *Boundary-Layer Meteorology*, *120*(1), 181–200. https://doi.org/10.1007/s10546-005-9035-3
Hicks, M., Sakay, R., & Joseph, E. (2015). The evaluation of a new method to detect mixing layer heights using lidar observations. *Journal of Atmospheric and Oceanic Technology*, *32*, 2041–2051. https://doi.org/10.1175/JTECH-D-14-00103.1
Huang, M., Gao, Z., Miao, S., Chen, F., LeMone, M. A., Li, J., et al. (2017). Estimate of boundary-layer depth over Beijing, China, using doppler lidar data during SURF-2015. *Boundary-Layer Meteorology*, *162*(3), 503–522. https://doi.org/10.1007/s10546-016-0205-2
IBGE (2019). IBGE Demographics Censuses (available at http://www.ibge.gov.br/).
Johansson, C., & Bergström, H. (2005). An auxiliary tool to determine the height of the boundary layer. *Boundary-Layer Meteorology*, *115*(3), 423–432. https://doi.org/10.1007/s10546-004-1424-5
Koracin, D., & Berkowicz, R. (1988). Nocturnal boundary-layer height: Observations by acoustic sounders and prediction in terms of surface-layer parameters. *Boundary-Layer Meteorology*, *43*, 65–83.
Kousky, V. E., & Gan, M. A. (1981). Upper tropospheric cyclonic vortices in the tropical South Atlantic. *Tellus*, *33*, 538–551. https://doi.org/10.3402/tellusa.v33i6.10775
Landulfo, E., Lopes, F. J., Mariano, G. L., Torres, A. S., de Jesus, W. C., Nakaema, W. M., et al. (2010). Study of the properties of aerosols and the air quality index using a backscatter lidar system and aeronet sunphotometer in the city of São Paulo, Brazil. *Journal of the Air and Waste Management Association*, *60*(4), 386–392. https://doi.org/10.3155/1047-3289.60.4.386
Landulfo, E., Papayannis, A., Artaxo, P., Castanho, A. D. A., De Freitas, A. Z., Souza, R. F., et al. (2003). Synergetic measurements of aerosols over São Paulo, Brazil using LIDAR, sunphotometer and satellite data during the dry season. *Atmospheric Chemistry and Physics*, *3*, 1523–1539. https://doi.org/10.5194/acp-3-1523-2003
Leclerc, M. Y., & Foken, T. (2014). *Footprints in micrometeorology and ecology* (1st ed.). Heidelberg, Germany, New York, USA, Dordrecht, the Netherlands, London, UK: Springer.
Lee, T. R., & De Wekker, S. F. J. (2016). Estimating daytime planetary boundary layer heights over a valley from rawinsonde observations at a nearby airport: An application to the page valley in Virginia, United States. *Journal of Applied Meteorology and Climatology*, *55*, 791–809. https://doi.org/10.1175/JAMC-D-15-0300.1
LeMone, M. A., Tewari, M., Chen, F., & Dudhia, J. (2012). Objectively determined fair-weather CBL depths in the ARW-WRF model and their comparison to CASES-97 observations. *Monthly Weather Review*, *141*(1), 30–54. https://doi.org/10.1175/mwr-d-12-00106.1
Lenters, J. D., & Cook, K. H. (1997). On the origin of the Bolivian High and related circulation features of the South American climate. *Journal of the Atmospheric Sciences*, *54*, 656–678. https://doi.org/10.1175/1520-0469(1997)054<0656:otootb>2.0.co;2
Liu, B., Ma, Y., Gong, W., Zhang, M., & Yang, J. (2018). Determination of boundary layer top on the basis of the characteristics of atmospheric particles. *Atmospheric Environment*, *178*, 140–147. https://doi.org/10.1016/j.atmosenv.2018.01.054
Liu, B., Ma, Y., Guo, J., Gong, W., Zhang, Y., Mao, F., et al. (2019). Boundary layer heights as derived from ground-based radar wind profiler in Beijing. *IEEE Transactions on Geoscience and Remote Sensing*, *57*(10), 8095–8104. https://doi.org/10.1109/tgrs.2019.2918301
Liu, S., & Liang, X. Z. (2010). Observed diurnal cycle climatology of planetary boundary layer height. *Journal of Climate*, *23*, 5790–5809. https://doi.org/10.1175/2010JCLI3552.1
Lotteraner, C., & Piringer, M. (2016). Mixing-height time series from operational ceilometer aerosol-layer heights. *Boundary-Layer Meteorology*, *161*(2), 265–287. https://doi.org/10.1007/s10546-016-0169-2
Lyra, A., Tavares, P., Chou, S. C., Sueiro, G., Dereczynski, C., Sondermann, M., et al. (2018). Climate change projections over three metropolitan regions in Southeast Brazil using the non-hydrostatic Eta regional climate model at 5-km resolution. *Theoretical and Applied Climatology*, *132*(1-2), 663–682. https://doi.org/10.1007/s00704-017-2067-z
Mahrt, L., Andre, J. C., & Heald, R. C. (1982). On the depth of the nocturnal boundary layer. *Journal of Applied Meteorology*, *21*, 90–92. https://doi.org/10.1175/1520-0450(1982)021<0090:otdotn>2.0.co;2
Melgarejo, J. W., & Deardorff, J. W. (1974). Stability functions for the boundary-layer resistance laws based upon observed boundary-layer heights. *Journal of the Atmospheric Sciences*, *31*, 1324–1333. https://doi.org/10.1175/1520-0469(1975)032<0837:rtfftb>2.0.co;2
Mishra, S. K., Rao, V. B., & Franchito, S. H. (2007). Genesis of the northeast Brazil upper-tropospheric cyclonic vortex: A primitive equation barotropic instability study. *Journal of the Atmospheric Sciences*, *64*, 1379–1392. https://doi.org/10.1175/jas3893.1
Mishra, S. K., Rao, V. B., & Gan, M. A. (2001). Structure and evolution of the large-scale flow and an embedded upper-tropospheric cyclonic vortex over northeast Brazil. *Monthly Weather Review*, *129*, 1673–1688. https://doi.org/10.1175/1520-0493(2001)129<1673:saeotl>2.0.co;2
Nair, K. N., Freitas, E. D., Sánchez-Ccoyllo, O. R., Silva Dias, M. A. F., Silva Dias, P. L., Andrade, M. F., & Massambani, O. (2004). Dynamics of urban boundary layer over São Paulo associated with mesoscale processes. *Meteorology and Atmospheric Physics*, *86*(1–2), 87–98. https://doi.org/10.1007/s00703-003-0617-7
Nieuwstadt, F. T. M. (1981). The steady state height and resistance laws of the nocturnal boundary layer: Theory compared with Cabauw observations. *Boundary-Layer Meteorology*, *20*, 3–17.
Oke, T. R. (1987). *Boundary Layer Climates* (2nd ed.). London: Matheuen.
Oliveira, A. P., Bornstein, R. D., & Soares, J. (2003). Annual and diurnal wind patterns in the city of São Paulo. *Water, Air, and Soil Pollution: Focus*, *3*, 3–15. https://doi.org/10.1023/A:1026090103764
Oliveira, A. P., Marques Filho, E. P., Ferreira, M. J., Codato, G., Ribeiro, F. N. D., Landulfo, E., et al. (2019). Assessing urban effects on the climate of metropolitan regions of Brazil—Implementation and preliminary results of the MCITY BRAZIL Project. (Under revision at the Theoretical and Applied Climatology).
Oliveira, A. P., Soares, J., Tirabassi, T., & Rizza, U. (1998). A surface energy-budget model coupled with a Skewed Puff model for investigating the dispersion of radionuclides in a sub-tropical area of Brazil. *Il Nuovo Cimento*, *21C*(6), 631–646.
Pal, S., Xueref-Remy, I., Ammoura, L., Chazette, P., Gibert, F., Royer, P., et al. (2012). Spatio-temporal variability of the atmospheric boundary layer depth over the Paris agglomeration: An assessment of the impact of the urban heat island intensity. *Atmospheric Environment*, *63*, 261–275. https://doi.org/10.1016/j.atmosenv.2012.09.046

Pournazeri, S., Venkatram, A., Princevac, M., Tan, S., & Schulte, N. (2012). Estimating the height of the nocturnal urban boundary layer for dispersion applications. *Atmospheric Environment*, *54*, 611–623. https://doi.org/10.1016/j.atmosenv.2012.02.024

Quan, J., Gao, Y., Zhang, Q., Tie, X., Cao, J., Han, S., et al. (2013). Evolution of planetary boundary layer under different weather conditions, and its impact on aerosol concentrations. *Particuology*, *11*, 34–40. https://doi.org/10.1016/j.partic.2012.04.005

Ribeiro, F. N. D., Oliveira, A. P., Soares, J., Miranda, R. M., Barlage, M., & Chen, F. (2018). Effect of sea breeze propagation on the urban boundary layer of the metropolitan region of Sao Paulo, Brazil. *Atmospheric Research*, *214*, 174–188. https://doi.org/10.1016/j.atmosres.2018.07.015

Sánchez, M. P. (2017). Investigação da camada limite planetária noturna na região metropolitana de São Paulo. Universidade de São Paulo (available in Portuguese at http://www.labmicro.iag.usp.br/publicacoes/Teses&Dissertacoes/Sanches_2017-INVESTIGACA_DA_CLU_NA_RMSP.pdf)

Sawyer, V., & Li, Z. (2013). Detection, variations and intercomparison of the planetary boundary layer depth from radiosonde, lidar and infrared spectrometer. *Atmospheric Environment*, *79*, 518–528. https://doi.org/10.1016/j.atmosenv.2013.07.019

Seibert, P., Beyrich, F., Gryning, S. E., Joffre, S., Rasmussen, A., & Tercier, P. (2000). Review and intercomparison of operational methods for the determination of the mixing height. *Atmospheric Environment*, *34*, 1001–1027. https://doi.org/10.1016/S1352-2310(99)00349-0

Seidel, D. J., Ao, C. O., & Li, K. (2010). Estimating climatological planetary boundary layer heights from radiosonde observations: Comparison of methods and uncertainty analysis. *Journal of Geophysical Research*, *115*, D16113. https://doi.org/10.1029/2009JD013680

Sorbjan, Z. (1989). *Structure of the atmospheric boundary layer*. Englewood Cliffs, NJ: Prentice-Hall.

Sorensen, J. H., Rasmussen, A., & Svensmark, H. (1996). Forecast of atmospheric boundary-layer height utilised for ETEX real-time dispersion modelling. *Physics and Chemistry of the Earth*, *21*, 435–439.

Steeneveld, G. J., van de Wiel, B. J. H., & Holtslag, A. A. M. (2007). Diagnostic equations for the stable boundary layer height: Evaluation and dimensional analysis. *Journal of Applied Meteorology and Climatology*, *46*, 212–225. https://doi.org/10.1175/JAM2454.1

Stull, R. B. (1988). *An introduction to boundary layer meteorology*. Dordrecht: Kluwer Academic Publishers.

Sun, X., Cook, K. H., & Vizy, E. K. (2017). The South Atlantic subtropical high: Climatology and interannual variability. *Journal of Climate*, *30*, 3279–3296. https://doi.org/10.1175/JCLI-D-16-0705.1

UNESCO (2017). United Nation Population Division (available at https://esa.un.org/unpd/wup/CD-ROM/)

Valença, R. L. (2013). Simulação numérica da evolução diurna da Camada Limite Planetária na Região Metropolitana de São Paulo usando modelo LES: Investigação do fluxo turbulento de calor latente. Universidade de São Paulo (available in Portuguese at http://www.labmicro.iag.usp.br/publicacoes/Teses&Dissertacoes/VALENCA_R_2013_DISSERTACAO_MESTRADO.pdf)

Velleman, P. F., & Hoaglin, D. C. (1981). *Applications, basics, and computing of exploratory data analysis*. Boston, MA: Duxbury Press.

Vemado, F., & Pereira Filho, A. J. (2016). Severe weather caused by heat island and sea breeze effects in the metropolitan area of São Paulo, Brazil. *Advances in Meteorology*, *8364134*. https://doi.org/10.1155/2016/8364134

Vickers, D., & Mahrt, L. (1997). Quality control and flux sampling problems for tower and aircraft data. *Journal of Atmospheric and Oceanic Technology*, *14*(3), 512–526.

Wang, X., & Wang, K. (2016). Homogenized variability of radiosonde-derived atmospheric boundary layer height over the global land surface from 1973 to 2014. *Journal of Climate*, *29*, 6893–6908. https://doi.org/10.1175/JCLI-D-15-0766.1

Willmott, C. J. (1981). On the validation of models. *Physic Geogr.*, *2*, 184–194.

World Meteorological Organization (2006). Guide to meteorological instruments and methods of observation. WMO-No. 8, Secretariat of the World Meteorological Organization-Geneva-Switzerland.

Wyngaard, J. C. (1990). Scalar fluxes in the planetary boundary layer theory, modeling and measurement. *Boundary-Layer Meteorology*, *50*, 49–75.

Wyngaard, J. C. (2010). *Turbulence in the Atmosphere*. Cambridge, UK: Cambridge University Press.

Yu, T. W. (1978). Determining the height of the nocturnal layer. *Journal of Applied Meteorology*, *17*, 28–33.

Zhang, Y., Gao, Z., Li, D., Li, Y., Zhang, N., Zhao, X., & Chen, J. (2014). On the computation of planetary boundary-layer height using the bulk Richardson number method. *Geoscientific Model Development*, *7*, 2599–2611. https://doi.org/10.5194/gmd-7-2599-2014

Zhang, Y., & Li, S. (2019). Climatological characteristics of planetary boundary layer height over Japan. *International Journal of Climatology*, *39*, 4015–4028. https://doi.org/10.1002/joc.6056

Zhang, Y., Seidel, D. J., & Zhang, S. (2013). Trends in planetary boundary layer height over Europe. *Journal of Climate*, *26*, 10,071–10,076. https://doi.org/10.1175/JCLI-D-13-00108.1

Zilitinkevich, S. S. (1972). On the determination of the height of the Ekman boundary layer. *Boundary-Layer Meteorology*, *3*, 141–145. https://doi.org/10.1007/BF02033914

Zilitinkevich, S. S., Esau, I., & Baklanov, A. (2007). Further comments on the equilibrium height of neutral and stable planetary boundary layers. *Quart. J. R. Met. Soc.*, *133*, 265–271. https://doi.org/10.1002/qj